January 2008

A Mathematical Model of Acute Response of Parathyroid Hormone to Changes in Plasma Ionized Calcium in Normal Humans

Rajiv P. Shrestha
University of Massachusetts Amherst, rshresth@engin.umass.edu

A MATHEMATICAL MODEL OF ACUTE RESPONSE OF PARATHYROID HORMONE TO CHANGES IN PLASMA IONIZED CALCIUM IN NORMAL HUMANS

A Thesis Presented

by

RAJIV P. SHRESTHA

Submitted to the Graduate School of the
University of Massachusetts Amherst in partial fulfillment
of the requirements for the degree of

MASTER OF SCIENCE IN MECHANICAL ENGINEERING

May 2008

Mechanical and Industrial Engineering

A MATHEMATICAL MODEL OF ACUTE RESPONSE OF PARATHYROID HORMONE TO CHANGES IN PLASMA IONIZED CALCIUM IN NORMAL HUMANS

A Thesis Presented

by

RAJIV P. SHRESTHA

Approved as to style and content by:

Yossi Chait, Co-chair

Christopher V. Hollot, Co-chair

Stuart Chipkin, Member

Moon Ki Kim, Member

Mario Rotea, Department Chair
Mechanical and Industrial Engineering

To Mom, Dad, Sudeep, Dilasha Didi and Suraj Dai.

ACKNOWLEDGMENTS

I would like to express my most sincere gratitude to my research advisor, Prof. Yossi Chait. My childhood dream of becoming both 'a doctor and an engineer' has materialized under his valuable mentorship. He provided me with all the freedom, the necessary tools, the resources, and the guidance that was crucial in exploring, what was to me, an unfamiliar research territory. I would like to extend my gratitude to my co-advisors, Prof. Christopher V Hollot, for providing me excellent guidance through the mathematical aspects of my research, and Prof. Stuart Chipkin for critical insights in the clinical aspects of my research. I am thankful to Prof. Moon K Kim for accepting to stay on my thesis defense committee in spite of his busy schedule. The thesis will be incomplete without thanking my lab-mate, Steve J Merrill for his great company in the lab and assistance in preparing the final draft of the thesis. I would like to thank my family and friends, near and far, for their good wishes, blessings and constant encouragement. I am thankful to National Science Foundation (NSF) for granting the NSF Award: # CMS-0556081, which supported my work in part.

ABSTRACT

A MATHEMATICAL MODEL OF ACUTE RESPONSE OF PARATHYROID HORMONE TO CHANGES IN PLASMA IONIZED CALCIUM IN NORMAL HUMANS

MAY 2008

RAJIV P. SHRESTHA

B.E., INSTITUTE OF ENGINEERING, PULCHOWK CAMPUS, KATHMANDU, NEPAL

M.S.M.E., UNIVERSITY OF MASSACHUSETTS AMHERST

Directed by: Professor Yossi Chait and Professor Christopher V. Hollot

A complex bio-mechanism, referred to as calcium homeostasis, regulates plasma ionized calcium (Ca^{++}) concentration in the human body to within a narrow physiologic range which is crucial for maintaining normal physiology and metabolism. Various metabolic disorders and pathologic conditions originate from acute and/or chronic disturbances/disorders in calcium homeostatic system. This system relies on numerous sub-systems which operate in different time-scales ranging from minutes to weeks. In this thesis we focus on a particular sub-system that operates on the time-scale of minutes; the dynamics involves the response of the parathyroid glands to acute changes in plasma Ca^{++} concentration. We develop a two-pool, linear time-varying model describing the dynamics of the sub-system. We show that this model can predict dynamics observed in clinical tests of induced hypo- and hyper-

calcemia in normal humans. In addition, we develop a new protocol for the construction of a Ca-PTH reverse sigmoid curve based on the mathematical model. This protocol removes deficiencies in current protocols in that the resulting curve is invariant with respect to the subject's axis dynamics and calcium clamp test dynamics.

TABLE OF CONTENTS

LIST OF TABLES

Table **Page**

LIST OF FIGURES

Figure **Page**

NOMENCLATURE

Parameters	**Values**	**Units**
PTH	Parathyroid hormone	-
PTC	Parathyroid cell	-
PTG	Parathyroid gland	-
PTH_P	PTH in plasma pool	-
PTH_C	PTH in PTC	-
Ca_P	Ionized calcium in plasma pool	-
25D	25 hydroxy Vitamin D	-
$25D_P$	25D in plasma pool	-
1,25D	1,25 dihydroxy Vitamin D	-
$1,25D_P$	1,25D in plasma pool	-
DNA	Deoxyribonucliec acid	-
RNA	Ribonucliec acid	-
mRNA	Messenger ribonucliec acid	-
VDR	Vitamin D receptor	-
CaR	Calcium receptor	-
x_1	Amount of parathyroid hormone in PTG pool	pmol
$x_{1,SS,N}$	Amount of normal PTH in PTG pool	pmol
$x_{1,SS,Max}$	Amount of maximal steady-state PTH in PTG pool	pmol
$x_{1,SS,Max}$	Amount of maximal steady-state PTH in PTG pool	pmol
$x_{1,SS,Min}$	Amount of minimal steady-state PTH in PTG pool	pmol
x_2	Amount of PTH in plasma pool	pmol
$x_{2,SS,N}$	Amount of normal PTH in plasma pool	pmol
$x_{2,SS,Max}$	Amount of maximal steady-state PTH in plasma pool	pmol
$x_{2,SS,Min}$	Amount of minimal steady-state PTH in plasma pool	pmol
Y_{max}	Peak value of PTH response	$pmolL^{-1}$
σ	Rate constant of change in plasma Ca^{++} concentration	min^{-1}
t_{max}	Time taken to reach Y_{max} by PTH response	min^{-1}

$Ca(t)$	Ionized calcium concentration in plasma pool	mmolL^{-1}
$Ca_{\mathrm{SS,N}}$	Normal Ionized calcium concentration in plasma pool	mmolL^{-1}
t	Time	min
τ	Half-life	min
τ_1	Half-life of PTH in PTG pool	min
τ_2	Half-life of PTH in plasma pool	min
λ	Decay rate constant	min^{-1}
λ_1	Decay rate constant of PTH in PTG pool	min^{-1}
λ_2	Clearance rate constant of PTH in plasma pool	min^{-1}
$\lambda_{\mathrm{Ca}}(\mathrm{t})$	secretion rate constant of PTH from PTG pool	min^{-1}
V	Volume	L

CHAPTER 1

INTRODUCTION

Calcium homeostasis refers to a complex bio-mechanism that regulates plasma ionized calcium (Ca^{++}) concentration in the human body to within a narrow physiologic range which is crucial for maintaining normal physiology and metabolism. Plasma Ca^{++} plays a vital role in normal functioning of muscles, nerves, platelets, neutrophils, and coagulation factors, cell growth, cell division, secretion of hormones and other regulators [1], and mineralization of bones [2]. This complex bio-system comprises numerous sub-systems interconnected via positive and negative feedback pathways.

Various metabolic disorders and pathologic conditions originate from acute and/or chronic disturbances/disorders in the calcium homeostasis. They can be caused by any one or a combination of the following factors: a) changes in plasma Ca^{++} levels and/or vitamin D levels by a physiologically significant amount, b) impaired synthesis and/or secretion of parathyroid hormone (PTH), and c) pathological conditions of parathyroid glands and kidneys. These disorders may affect normal bone remodeling process causing various metabolic bone diseases, such as osteoporosis, a major public health concern in the United States [3, 4], besides causing many other abnormalities and disease conditions (eg., primary and secondary hyperparathyroidism).

The present understanding of calcium homeostasis and its disorders is based on the traditional approach of biological and medical science which involves discovering various signaling pathways, identifying critical bio-markers, and employing statistical analysis. However, calcium homeostasis is a sophisticated bio-system where numerous sub-systems interact at

different time-scales. A perturbation in one sub-system has corresponding effects in the interconnected sub-systems and these in turn have effects on the other sub-systems. These cascade-effects propagate in positive and negative feedback pathways in multiple directions. It becomes impractical, if not impossible, to keep track of all of these interactions in order to derive an understanding of the bio-system as a whole using the traditional approach. Systems biology, an emerging science, relies on the integration of mathematical models for individual sub-systems into a single model, enabling us to study the effects of disturbances in the various inputs, pools and processes of the overall bio-system [5, 6].

We took the systems biology approach in our overall calcium homeostasis modeling efforts. We first developed a qualitative model of the overall bio-system. Based on this qualitative model, substantial progress was made towards the development of a mathematical model (not presented in this thesis). However, during this process we realized that existing models for a very important aspect of calcium homeostasis, the acute dynamical interaction between plasma Ca^{++} and PTH (called the Ca-PTH axis for ease of notation) appeared deficient. To address this issue we decided to focus our research goal only on this axis of the bio-system.

The thesis is organized as follows. In Chapter 2, we present a detailed qualitative model of overall calcium homeostasis in a normal human, and explain why the Ca-PTH axis can be isolated from the overall bio-system. In Chapter 3, we develop a mathematical model of the acute Ca-PTH axis dynamics. In Chapter 4, we address the inconsistency in current procedures for deriving the calcium-PTH reverse sigmoid curve. This curve could potentially be used as an important bio-marker of diseases disrupting calcium homeostasis and to assess the effectiveness of treatment protocols, based on the mathematical model developed. The conclusions are given in Chapter 5.

The specific contributions of this thesis work are:

1. A new mathematical model describing the response of plasma PTH to acute changes in plasma Ca^{++} concentration in normal humans has been developed. This model can successfully predict dynamics observed in clinical tests of induced hypo- and hypercalcemic clamp tests.

2. A new method of generating Ca-PTH reverse sigmoid curve has been formulated. The resulting curve properties are independent of the manner by which the induced calcemic clamp test is conducted.

CHAPTER 2

QUALITATIVE MODEL OF CALCIUM HOMEOSTASIS

A detailed qualitative model describing the interactions between various components and signalling pathways of calcium homeostasis is presented in this chapter. We begin by describing the major pools and fluxes of calcium next.

2.1 Major pools and fluxes

The intestine, bone, kidney, and plasma are the four major pools of Ca^{++} in the human body. There is about 1-2 kg of calcium in a healthy adult, most of which (99%) is in the form of hydroxypatite crystals in teeth and bones [7]. Of the remaining, 50% constitutes the ionized or 'free' calcium in plasma, 40% is bound reversibly to proteins, and 10% is complexed with citrate and phosphate [1]. The average total plasma calcium concentration in the human body is 2.1-2.6 mmol/L [8]. At normal physiological state, about 1.1-1.3 mmol/L is ionized calcium, 0.9-1.1 mmol/L is protein-bound calcium, 0.18 mmol/L is complexed calcium and 180 nmol/L is intracellular free calcium [8]. The ionized form of calcium, which is just 0.5% of the total body calcium, is metabolically active [1] and tightly regulated by the homeostatic system. The condition when Ca^{++} level falls below the normal range is called *hypocalcemia* and the condition when it climbs above the normal range is called *hypercalcemia*.

An overall daily Ca^{++} balance in the plasma of a healthy adult is maintained by fluxes of calcium between the plasma and the intestine, bone and kidney as shown in Figure 2.1.

Intestine receives calcium from the external environment through diet. A normal daily diet contains about 1,000 mg of calcium. During the process of digestion only about 300

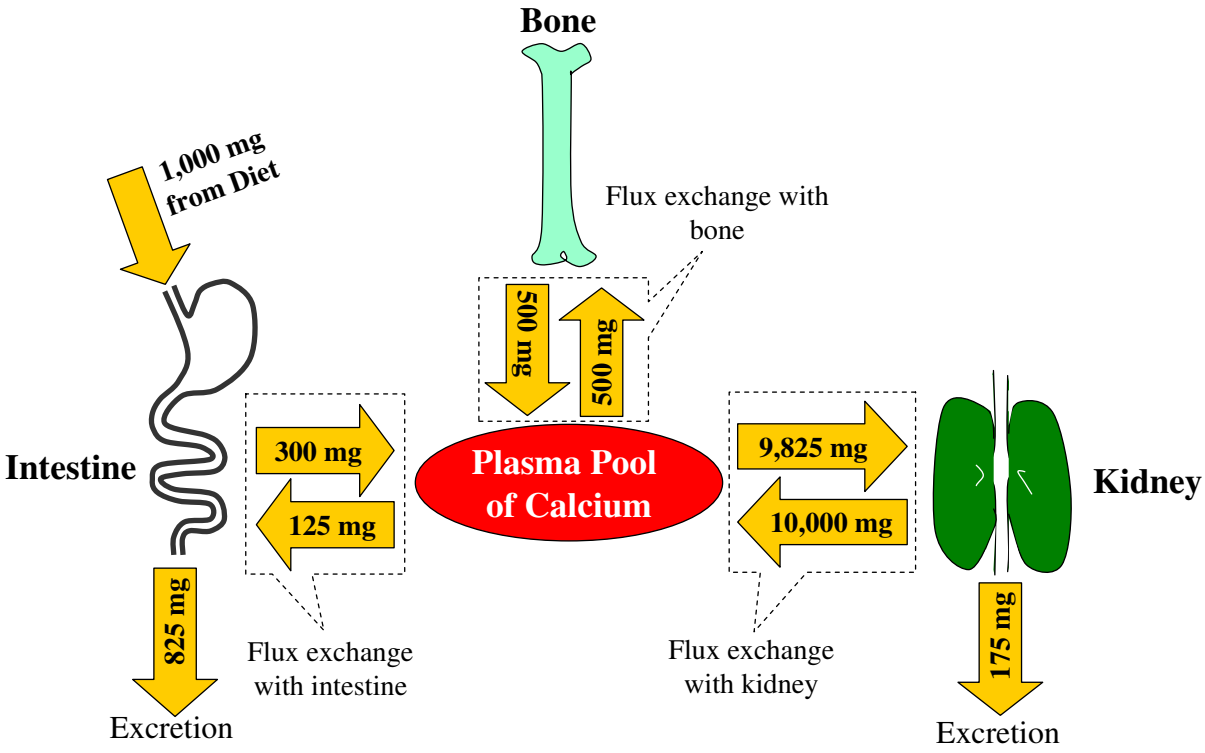

Figure 2.1. Daily calcium balance in a normal adult. The arrows show the direction of flux. Numerical values from [9].

mg are absorbed from the intestine into the plasma and roughly 125 mg are effluxed back into the intestine, which is cleared out through fecal excretion along with the unabsorbed fraction. Hence, the net dietary uptake of calcium into the plasma pool is 175 mg. There is an exchange of 500 mg of calcium to and from the bone with the plasma but the net exchange is zero assuming that in the time-scales of minutes to hours there is no change in bone mass. On a daily basis, 10,000 mg of calcium are ultra-filtered out of the plasma into nephrons in the kidney, where about 9,825 mg of calcium are reabsorbed. The net removal of calcium via the kidney is 175 mg per day, which is excreted in urine. Thus, the additional dietary calcium that enters into the circulation is excreted out and a normal plasma calcium concentration is maintained.

The flux exchange described above is actively regulated by two chief hormones: the metabolically active form of vitamin D and PTH. The metabolism and regulation of vitamin D and PTH are presented in the next sections, respectively.

2.2 Vitamin D metabolism and regulation

The general steps in the metabolism of vitamin D are shown in Figure 2.2 (the presentation here follows the detailed exposition in [10]). There are two sources of vitamin D in the human body: daily diet and skin. Daily diet provides vitamin D_2 (ergocalciferol) and

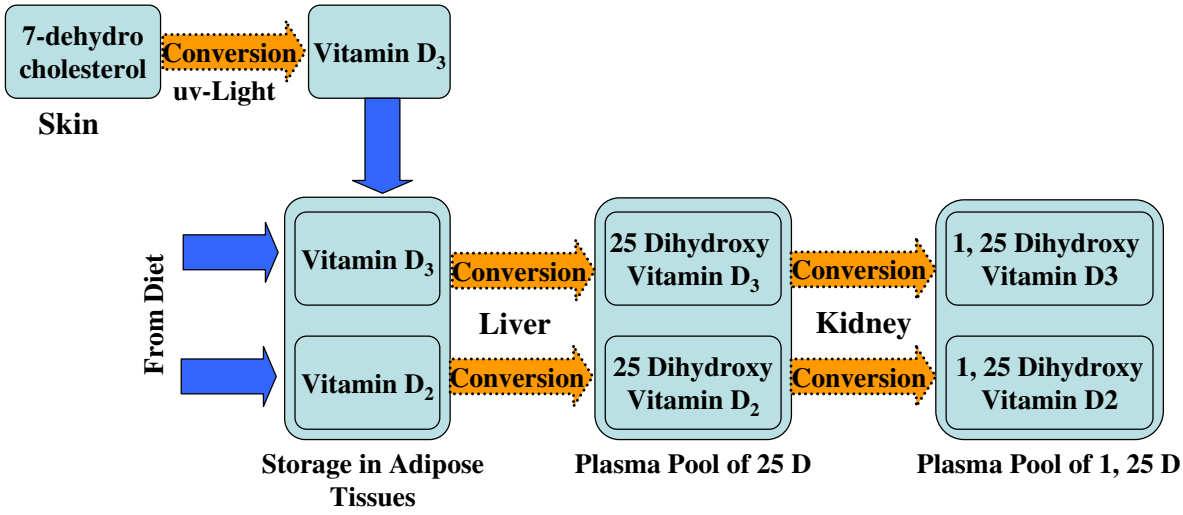

Figure 2.2. The general steps in vitamin D metabolism. Dotted arrows mean conversion and solid arrows mean transportation.

vitamin D_3 (cholecalciferol), whereas in skin, 7-dehydrocholesterol is converted into vitamin D_3 by exposure to uv-light. The biological actions of both forms of vitamin D is considered to be the same, hence, the term vitamin D is used to denote both forms in this work. Vitamin D does not circulate for long in the blood stream. It is immediately taken up by

adipose tissue for storage or by liver for 25-hydroxylation to form 25 hydroxy vitamin D[1]. 1,α hydroxylation of 25D occurs in the kidney to form the metabolically active 1,25 dihydroxy vitamin D[2]. In humans, tissue storage of vitamin D can last for months or even years. 25D is the major circulating form of vitamin D.

In a normal individual, there is an ample supply of Vitamin D to plasma directly from diet, skin, and storage in the adipose. The conversion of vitamin D to 25D in the liver is only loosely regulated [10]. However, the conversion of 25D to 1,25D in the kidney is tightly regulated by renal α hydroxylase enzyme and it has been established that the kidney is the major source of the circulating pool of 1,25D [10]. For our modeling purpose, the different steps in the vitamin D metabolism process have been lumped into a high-level schematic diagram as shown in Figure 2.3. Next, we present the bio-synthesis and secretion of PTH and their regulations.

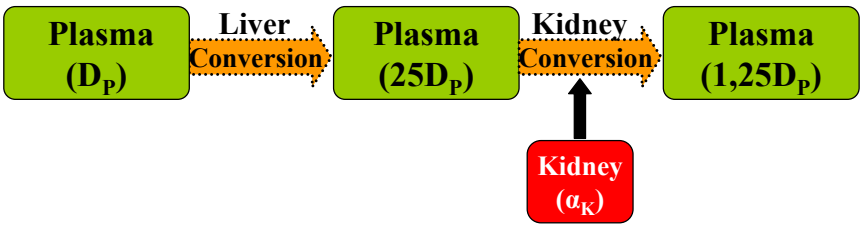

Figure 2.3. A high-level schematic diagram of the major steps in the metabolism of vitamin D and its regulation. The darkened solid arrow indicates stimulation.

2.3 PTH bio-synthesis and secretion and their regulation

There are four parathyroid glands, each weighing 40 mg on average, located adjacent to the thyroid gland in the neck [8] as shown in Figure 2.4(a). The chief cells, shown in

[1]We use 25D to denote 25 hydroxy vitamin D.

[2]We use 1,25D to denote 1,25 dihydroxy vitamin D.

Figure 2.4(b), are the predominant cells in the parathyroid glands [11]. PTH is synthesized

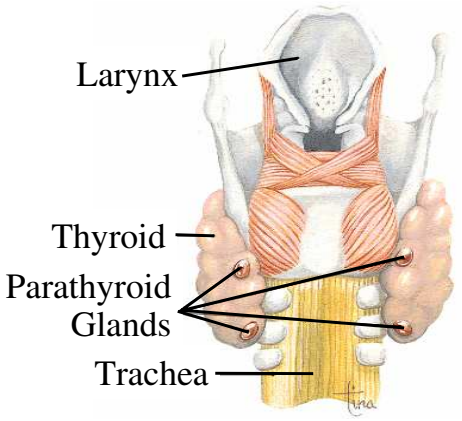

(a) Anatomy of the parathyroid glands. Reproduced from [12].

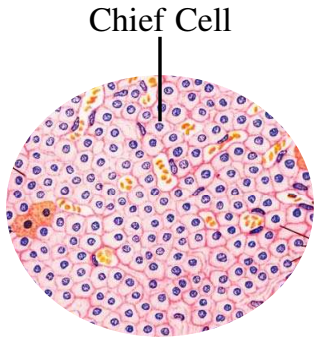

(b) Histology of the parathyroid gland. Stain: Hematoxylin-eosin.550x. Reproduced from [13].

Figure 2.4. Anatomy and histology of parathyroid glands.

and stored in the cytoplasmic vesicles of the chief cells. Normally, only about 20% of the cell population is actively secreting PTH [11]. Next, a simple understanding of these steps involved is presented based on [14, 15]. Figure 2.5 summarizes the steps.

The first step in the biosynthesis of PTH is the *transcription* process in which genetic information is transferred from the DNA (Deoxyribonucleic acid) to a pre-mRNA (pre-messenger ribonucleic acid) in the nucleus of the parathyroid cell. The *post-transcriptional* process follows. The pre-mRNA matures into an mRNA that is transported to the cytoplasm, the process being called *transportation*. The next step is the *translation* where the genetic information in the mRNA is translated into a specific polypeptide, a larger precursor of PTH, called pre-proPTH containing 115 amino acids. This process occurs in the endoplasmic reticulum-bound polyribosomes. The pre-proPTH is then cleaved in the rough endoplasmic reticulum to produce a 90 amino acid intermediate precursor of PTH called proPTH. This

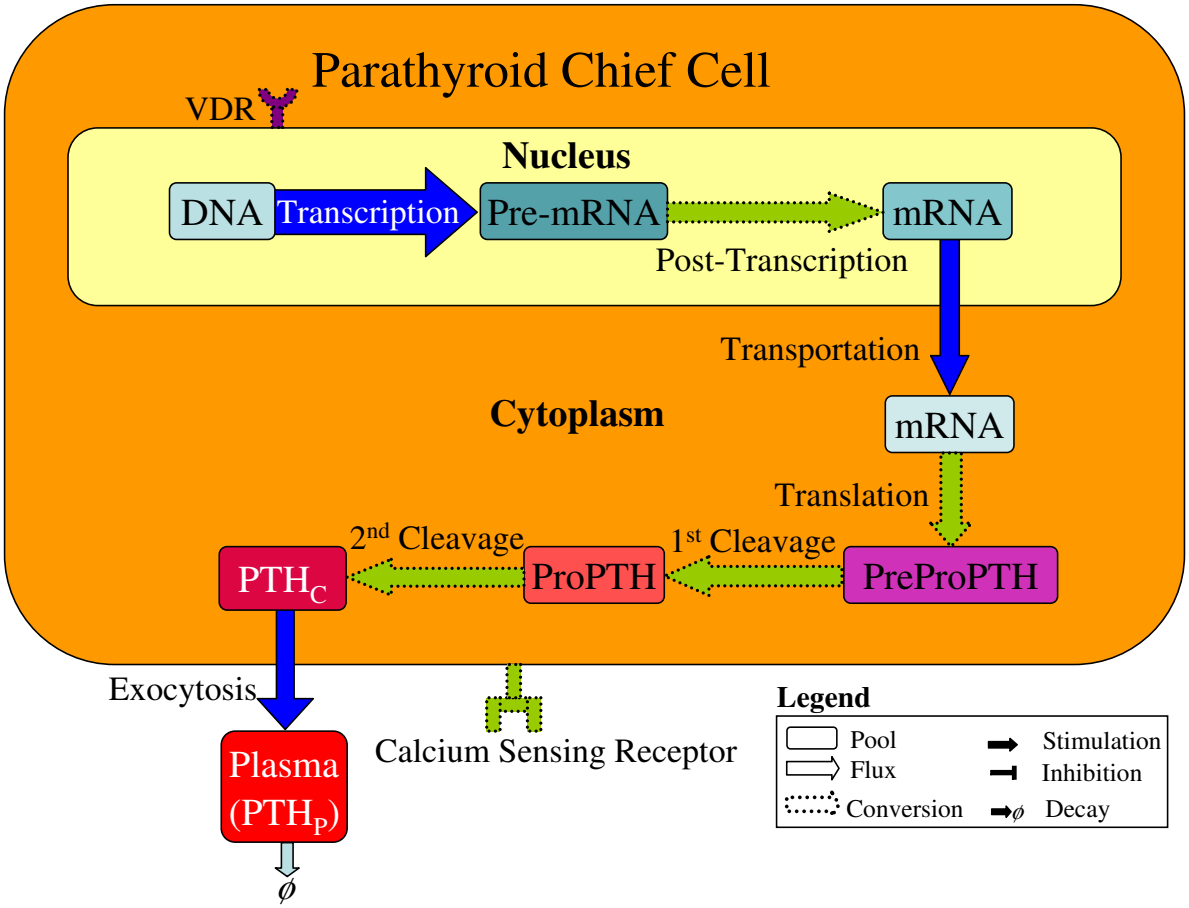

Figure 2.5. A schematic diagram describing various steps involved in PTH bio-synthesis inside a parathyroid chief cell. PTH thus synthesized is stored in vesicles inside the cells. PTH is secreted from the cells by exocytosis process.

process is called *first cleavage*. The *second cleavage* occurs in the golgi complex in the cytoplasm to finally produce the PTH which accumulates in the vesicles. In response to secretory stimulus caused by decrease in plasma Ca^{++} concentration to calcium sensing receptors (CaR) on the cell membrane [16], the membrane of the storage vesicle fuses with the cell membrane and PTH is released from the cell into circulation. This process is called *exocytosis*.

PTH bio-synthesis is regulated by plasma 1,25D during the transcriptional process [17] and by Ca^{++} during post-transcriptional process [18] as depicted in the Figure 2.6. The 1,25D form of vitamin D, with the plasma half-life of 12 to 15 hours [1], regulates the long-term parathyroid secretion function. It has been termed as a day-to-day regulator of calcium

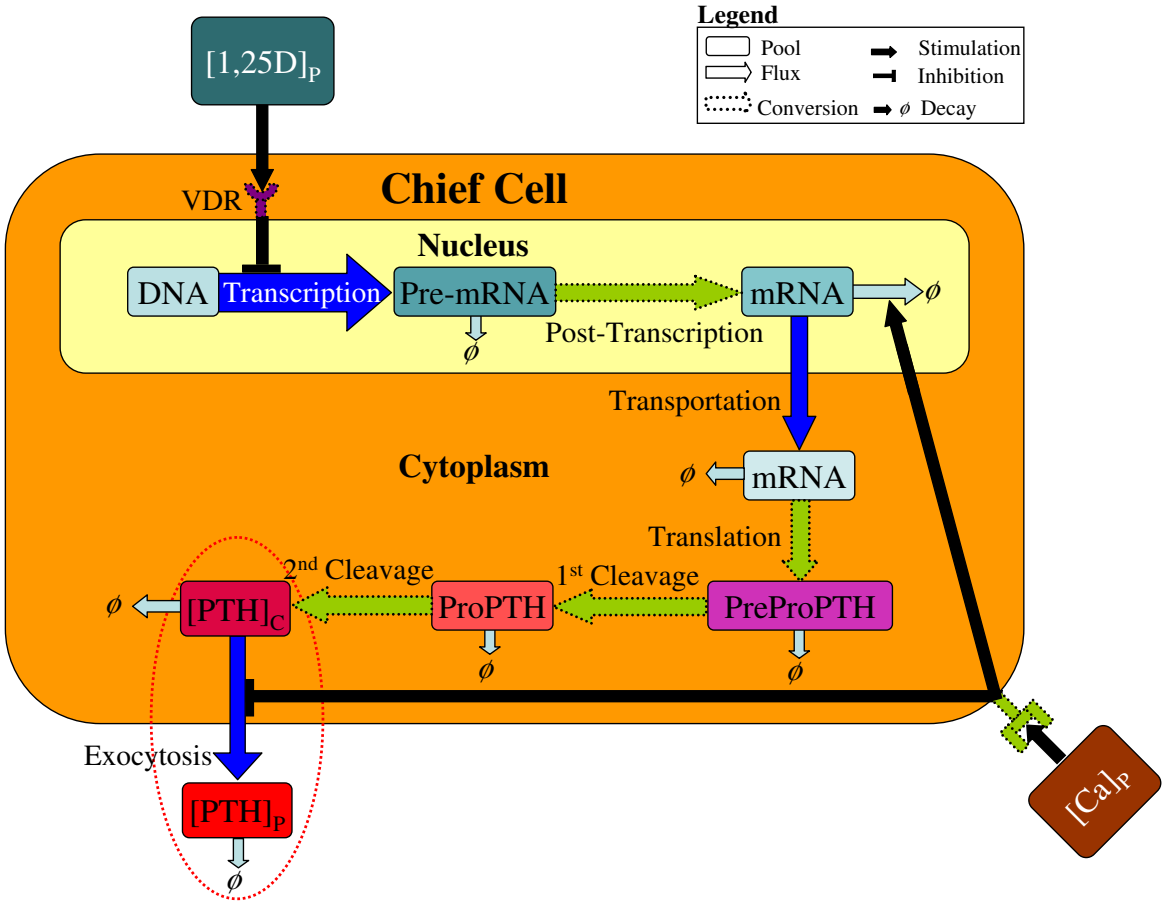

Figure 2.6. A schematic diagram showing the regulation of PTH bio-synthesis and secretion by 1,25D and calcium.

homeostasis [1]. Higher concentrations of 1,25D inhibit the transcription of the PTH gene [17] through signalling from the nuclear [8] vitamin D receptor (VDR). The effect occurs within 2 hours [1]. A decrease in PTH mRNA levels to less than 4% of controls was observed within 48 hours in rats that were injected with amounts of 1,25D which did not increase

their calcium levels [17]. The time-scale of this regulation of PTH synthesis by 1,25D cannot be pin-pointed. However, a time-scale of hours to days can be assumed based on [1, 17, 19]. Plasma Ca^{++} regulates PTH bio-synthesis during the post-transcriptional process. The regulation occurs by affecting the mRNA stability [18]. An increase in plasma Ca^{++} concentration decreases the overall PTH bio-synthesis by degrading the mRNA faster. Conversely, a decrease in plasma Ca^{++} concentration increases the overall PTH bio-synthesis by increasing the nuclear mRNA half-life. No known major regulatory effects have been observed at the translational and post-translational levels [14]. The time-scale of this regulation has been suggested to range from hours to days in [1, 14].

The regulation of exocytosis in response to changes in plasma Ca^{++} levels occurs strictly by signaling pathways involving calcium sensing receptors (CaR) located on the cell membrane of the chief cells of the parathyroid glands [16]. An increase in the plasma Ca^{++} concentration results in a decrease in PTH secretion. Conversely, a decrease in the plasma Ca^{++} concentration results in an increase in PTH secretion. The time-scale of the parathyroid gland's response to varying plasma Ca^{++} concentrations ranges from seconds to minutes [20, 16]. In our qualitative model of the calcium homeostasis the above described 1,25D and the plasma Ca^{++} concentration signaling pathways have been lumped together in terms of an overall effect on the exocytosis. Next, we put together the descriptions presented in Sections 2.1-2.3 to form a qualitative model of plasma calcium homeostasis.

2.4 Qualitative model of plasma calcium homeostasis

The plasma calcium pool size is maintained by a flux balance with the intestine, bone, and kidney. The influx of calcium from the intestine consists of both actively- and passively-regulated channels, whereas the efflux to the intestine is mainly due to passive transportation (Figure 2.7(a)). The efflux to the kidney involves ultrafiltration, where the filtration occurs

under high pressure in the glomerular capillaries of the kidney. The influx from the kidney involves a passive diffusion and an active reabsorption by the nephrons.

A decrease in the plasma Ca^{++} concentration acutely stimulates (a rise in the plasma Ca^{++} concentration inhibits) PTH secretion by exocytosis from the parathyroid cells in a time-scale of minutes [16]. In the time-scales of hours to days, a decrease in plasma Ca^{++} concentration increases (a rise in the plasma Ca^{++} concentration decreases) bio-synthesis of PTH in the parathyroid cells [14]. PTH in turn stimulates bone calcium resorption and active renal reabsorption of calcium. PTH also upregulates production of renal α hydroxylase enzyme in the kidney which upregulates conversion of 25D into 1,25D in the kidney. 1,25D in turn upregulates active intestinal calcium absorption and active renal calcium reabsorption. It also downregulates PTH bio-synthesis in the parathyroid cells and production of the renal α hydroxylase enzyme, resulting in the downregulation of its own production. These pathways are shown in Figure 2.7(b).

1,25D and PTH play important roles in regulating bone formation and resorption processes [8]. This results in the addition or removal of calcium from the plasma pool and the transportation of it to and from the bone. This process, of course, plays an important role in plasma calcium homeostasis. In fact, the bone acts as a big reservoir to supply calcium to the plasma in case of need. Though the exact function of 1,25D and PTH in the bone remodeling process is not well understood, it has now been generally accepted that 1,25D upregulates calcium trapping for bone formation [8] and an intermittent rise in PTH helps in a net positive bone formation [21, 22, 23] resulting in a net flux of calcium from plasma to bone. A lack of 1,25D and continuous rise in PTH upregulates bone resorption resulting in a net flux of calcium to the plasma. Phosphate in high concentrations stimulates PTH secretion and PTH upregulates phosphate clearance through the kidney. The effect of phosphate on the parathyroid gland is independent of plasma Ca^{++} and vitamin D [18]. Thus, the phosphate pool is not included in the present model.

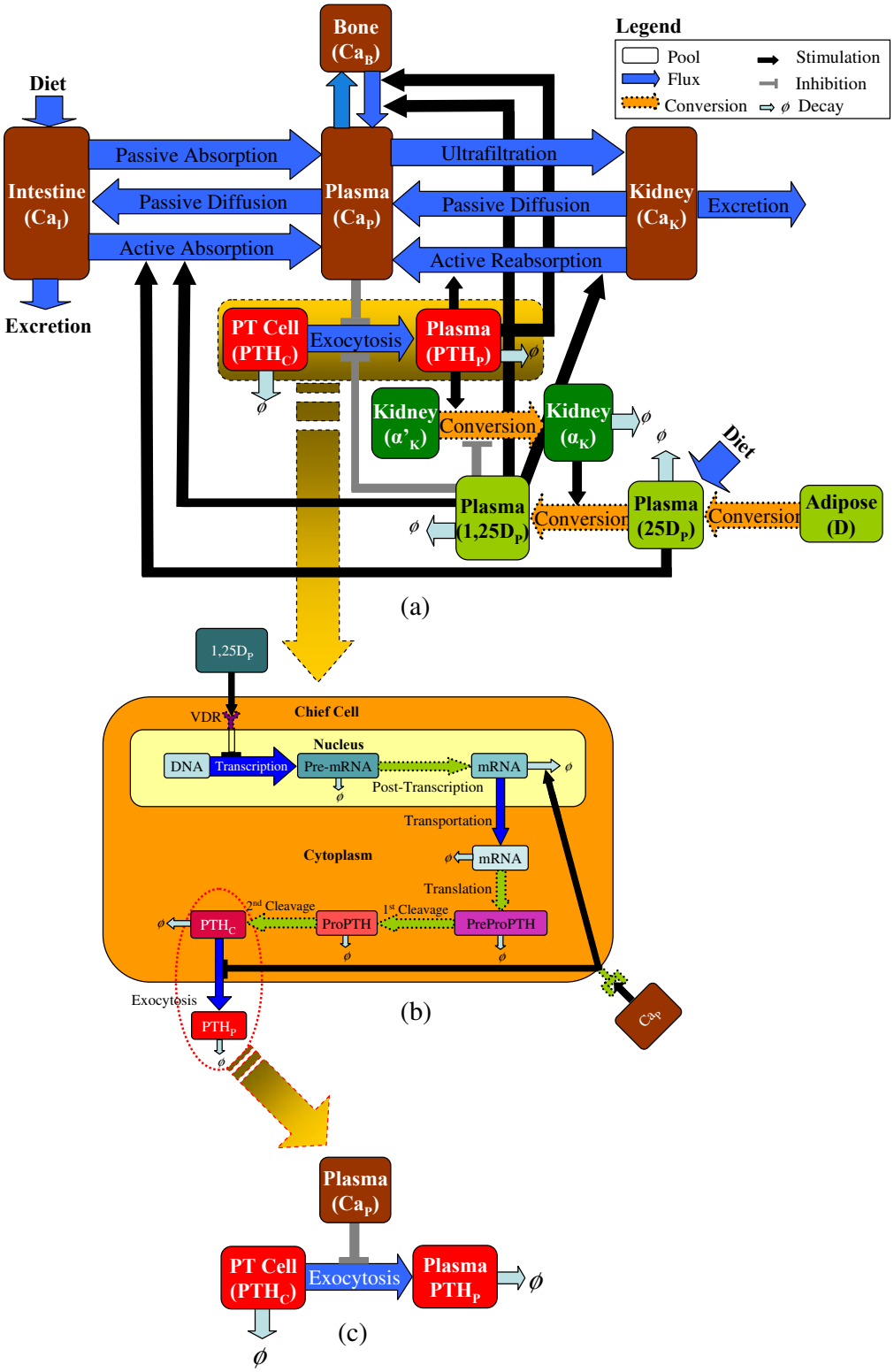

Figure 2.7. A qualitative model of plasma calcium homeostasis.

The response of the parathyroid glands to acute changes in plasma Ca^{++} concentration occurs in time-scales of seconds to minutes [16] which involves the exocytosis process. Because regulation of PTH bio-synthesis by plasma Ca^{++} and 1,25 D in the chief cells and all other signaling pathways in the calcium homeostatic system run in the time-scales of hours to days [18, 17], it is feasible to study the acute response of plasma PTH to changes in the plasma Ca^{++} separately from the overall system. We refer to this isolated sub-system (shown in Figure 2.7(c)) of the overall bio-system as the Ca-PTH axis from here on. Given that a reasonable amount of information is available about this axis, this thesis focuses on the development of a mathematical model for this axis, which is presented next in Chapter 3.

CHAPTER 3

A MATHEMATICAL MODEL OF THE CA-PTH AXIS

In this chapter we develop a model describing the response of PTH to acute changes in plasma Ca^{++} concentration (Ca-PTH axis) in humans. To fully appreciate this model, we first present a literature review of relevant published models.

3.1 Literature review

Our literature survey unraveled numerous models of calcium homeostasis of varying degrees of details. The earlier works are theoretical or have utilized data from animals and birds whereas the recent investigations have utilized data from humans. With the discovery of various receptors and ligands involved in the signalling pathways within individual sub-systems, the understanding of the details of calcium homeostasis has progressed substantially. Hence, most of the recent studies have focussed on modeling particular sub-systems of the calcium homeostasis, e.g. Ca-PTH axis [19, 20] and bone remodeling process [21, 22, 24].

One of the earliest works relevant to mathematical modeling of calcium homeostasis dates back to 1963 [25]. A theoretical approach of modeling calcium metabolism was presented. A central blood calcium pool with a bidirectional calcium flux exchange with both the skeleton and intestine and a unidirectional flux of calcium to urine were considered. Two schemes of calcium metabolism were presented. Various options were suggested for the collection of data required for parametrization of the model. The roles of regulating hormones were not included in the model.

Although the role of PTH in the acute regulation of plasma calcium levels was clearly established as early as 1959 [26] it seems to have been incorporated in a mathematical model for the first time in 1965 [27]. A model for the regulation of the blood calcium level in rats by bone metabolism was presented in this paper. It concluded that feedback systems with an integral control due to parathyroid hormone for a normal rat and a proportional control for a thyro-parathyroidectomized rat can explain the response of bone metabolism to changes in blood calcium levels.

Calcium homeostasis based on negative feedback control involving a proportional control by PTH during hypocalcemia and by calcitonin during hypercalcemia was suggested in [28]. Linear relationships between PTH secretion and calcium concentration with a negative slope and between calcitonin secretion and calcium concentration with a positive slope were assumed. A very simplified model of the Ca-PTH axis in dogs was presented in [29]. Experimental results from normal and thyro-parathyroidectomized dogs were utilized to calculate model parameters. It was assumed that the action of PTH is limited only to the resorption of bone and that its effects in the regulation of fluxes to and from the kidney and intestine are negligible at steady-state.

A theoretical, quasi-linear, lumped-parameter model for calcium homeostasis for mammals based on data from different animals, eg., dogs, rats, rabbits and pigs appears in [30]. PTH and calcitonin were assumed to be the prime hormones. Linear relationships were assumed between plasma calcium and both plasma calcitonin and plasma PTH. Finally, due to lack of data to validate the model, it only suggested possible experiments to obtain data to parameterize the model.

A general mathematical model for calcium homeostasis in birds was presented in [31]. The roles of PTH and 1,25D as regulating hormones for different calcium fluxes between bone, kidney, intestine, and plasma were taken into consideration. A calcium pool, a PTH hormone pool, and a 1,25D pool in the plasma, and a 1,25D pool in the intestine were

considered. A part of the intestinal flux of calcium was assumed to be regulated by 1,25D and a part of the bone flux of calcium was assumed to be regulated by PTH. The model also considered the regulation of renal hydroxylase enzyme by PTH, which in turn regulates the conversion of 25D to 1,25D. An extension to this model was presented in [32] which included the effects of body growth and energy intake models for chicks. This model utilized the reverse sigmoidal relationship between PTH secretion and plasma Ca^{++} concentrations presented in [33].

The first conclusive study demonstrating the nonlinear nature of the relationship between PTH secretions and plasma Ca^{++} level in a bovine, normal human, and pathological human parathyroid tissue in vitro was presented in [33]. A reverse sigmoidal model bearing four parameters representing various aspects of the secretion dynamics was presented in the paper. Further details on this model can be found in Chapter 4.

A proportional-integral feedback control structure was utilized to develop a dynamical model for calcium homeostasis in healthy dairy cows for longer time-scale of days in [34]. The proportional-integral feedback control was realized by assuming the production of 1,25D to be proportional to PTH concentration. Nonlinearities were introduced in the form of a saturation function in the relationships between: 1) PTH and calcium transportation from the bone to plasma, and 2) plasma Ca^{++} concentration and calcium transport from the intestine. These were used to study calcium homeostatic disorder and breakdown in dairy cows called parturient paresis or milk fever which occasionally affects them after calving. The results suggested that a reduction in bone remodeling reaction to PTH may cause milk fever. Moreover, for the breakdown to occur this reduced responsiveness must be accompanied by reduced gut motility.

A relatively recent attempt to model plasma calcium homeostasis consisting of separate pools of calcium, phosphate, PTH, calcitriol in plasma, intracellular phosphate, and parathyroid gland mass was presented in [35]. The exchangeable pools of calcium and phosphate

in bone were introduced to model flux exchange between the plasma and bone. Similarly, a renal 1,α hydroxylase pool, a phosphate pool, and an intestinal calcium pool were utilized to capture the dynamics involving the kidney and the intestine. Clinical data from a renal failure case was compared with simulation results with a favorable match. Generally speaking this model seems to have incorporated all the important aspects and recent understanding of calcium homeostasis and signalling pathways. However, this model cannot predict the observed Ca-PTH dynamics for short time-scales of less than 10 minutes. This becomes evident by comparing simulation results presented in the paper with clinical data for shorter time-scales presented in [20]. Moreover, the fact that the model uses a single PTH pool rules out the possibility of achieving dynamics observed in clinical data. A mathematical proof of the deficiency of the single PTH pool model will be presented in Section 4.4. Short time-scale dynamics may be important in an overall model of plasma calcium homeostasis, especially when we incorporate the interaction with bone because the intermittent change in PTH levels helps in net positive bone formation [21, 22, 23]. A brief review of the two mathematical models that capture short time-scale Ca-PTH interaction are discussed next.

3.1.1 Ca-PTH axis models

A multi-parameter deconvolution analysis method suggested in [36] was used to study the tonic and pulsatile nature of PTH secretion in normal humans in [37]. A *two-pool, linear, time-invariant* (LTI) model was arbitrarily assumed to represent the Ca-PTH axis. The model was parameterized using the hypo- and hyper-calcemic clamp test data separately. The parameterized models were used to estimate the tonic and pulsatile PTH secretion.

For the first time, [19] utilized the biological events in the process of PTH secretion to derive a two-pool model of Ca-PTH dynamics for short time-scales (in minutes). Two PTH pools, one in the parathyroid cells and the other in the blood, were considered. An important simplifying assumption that the change in calcium occurs instantaneously was

used to render the model into an LTI system. The presentation in [19] differs from the ones in [20, 37] in the respect that it utilizes the biological events to explain the origin of the model. This model, parameterized based on a hypocalcemic clamp test, matched the test results. Nevertheless, we note that the assumption of an instantaneous change in plasma calcium levels is not expected to hold in practice. The ability of this model to predict dynamics of a hypercalcemic clamp test was not explored. Next, we present some clinical observations on the Ca-PTH axis.

3.2 Clinical observations

A clinical protocol, referred to as an induced calcemic clamp test, is typically employed to study the status of the Ca-PTH axis. During an induced hypocalcemic clamp test, plasma Ca^{++} concentration is decreased by an intravenous infusion of sodium citrate. Similarly, during an induced hypercalcemic clamp test, plasma Ca^{++} concentration is increased by an intravenous infusion of calcium gluconate [20, 38, 39, 40, 41, 42]. Plasma Ca^{++} concentration and the corresponding plasma PTH concentration are measured at frequent time intervals. Both hypo- and hyper-calcemia can be induced at a fast or a slow rate depending upon the rate of infusion of sodium citrate or calcium gluconate, respectively. Examples of clamp tests induced slowly [40] or rapidly [20] can be seen in Figure 3.1 and Figure 3.2, respectively. For ease of illustration and analysis, typical time profiles of plasma Ca^{++} and PTH concentrations for induced hypo- and hyper-calcemic clamp tests are depicted in Figure 3.3 and Figure 3.4, respectively. Next, we present the dynamical model development.

3.3 Model Development

Based on the description of the PTH secretion process and its regulation in Sections 2.3 and clinical observations in Section 3.2 we consider two pools of PTH: one in the parathyroid

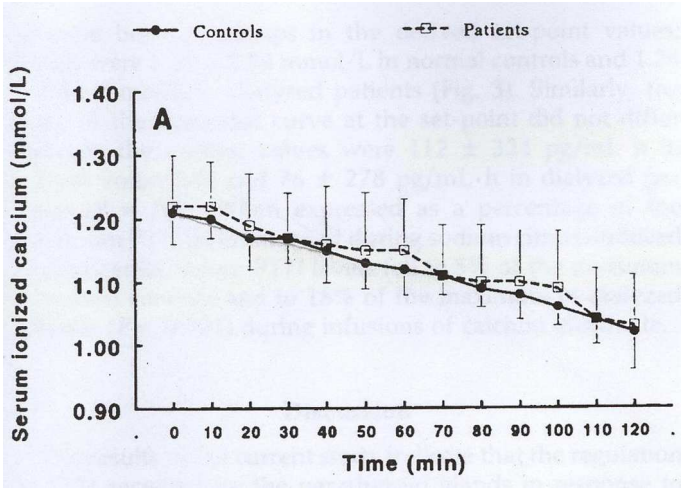

(a) Induced hypocalcemia.

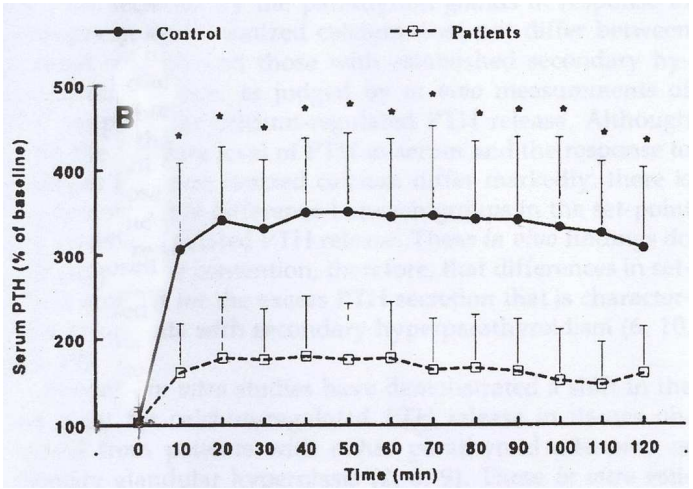

(b) PTH response for induced hypocalcemia.

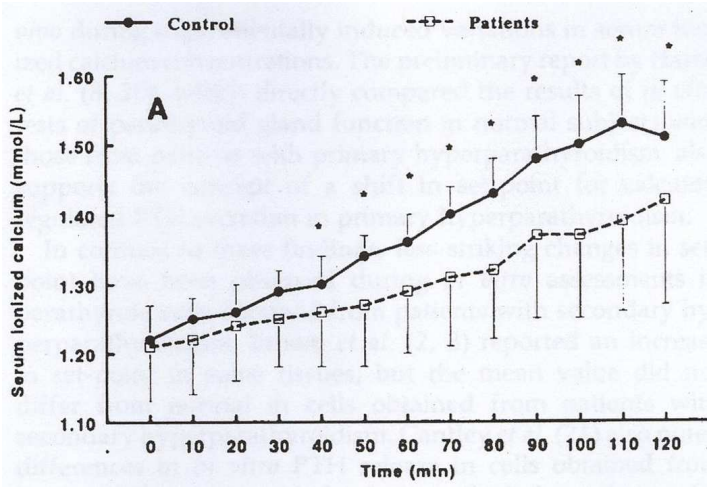

(c) Induced hypercalcemia.

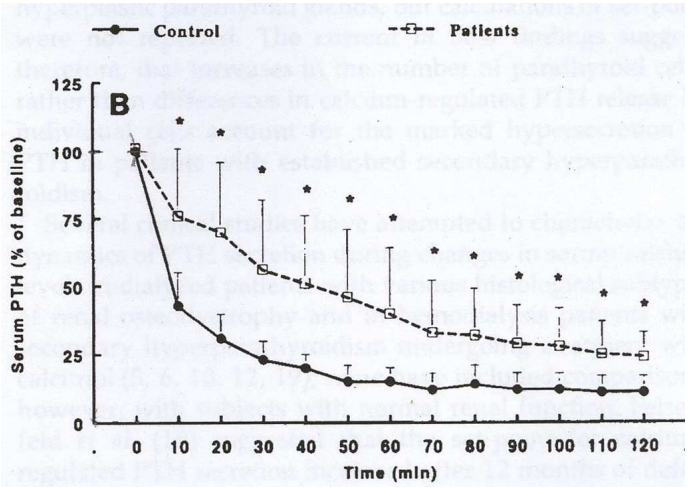

(d) PTH response for induced hypercalcemia.

Figure 3.1. An example of slowly induced calcemic clamp test. Solid dots represent data of healthy subjects. Squares represent data of diseased subjects. Scanned from [40].

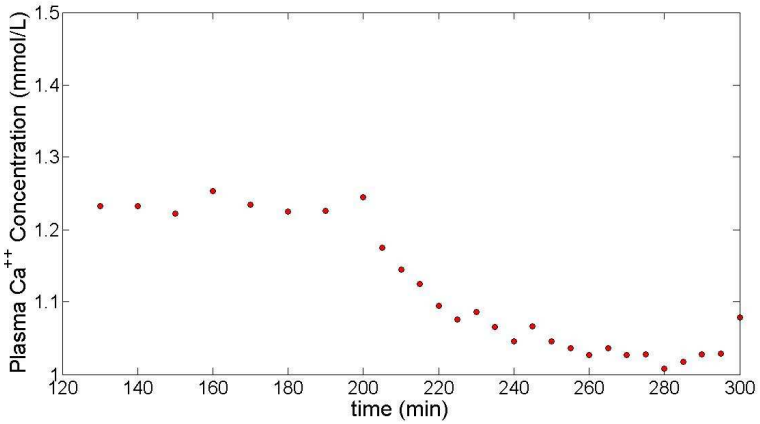

(a) Induced hypocalcemia.

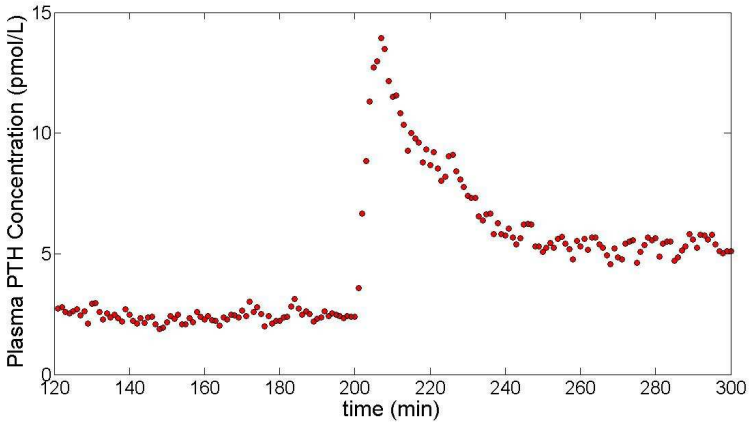

(b) PTH response for induced hypocalcemia.

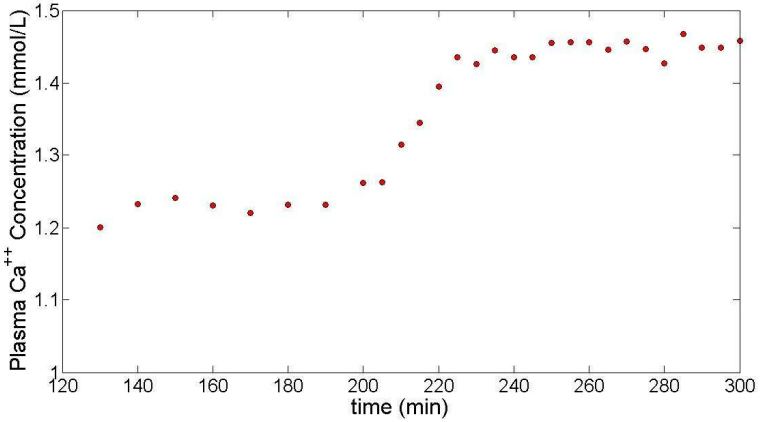

(c) Induced hypercalcemia.

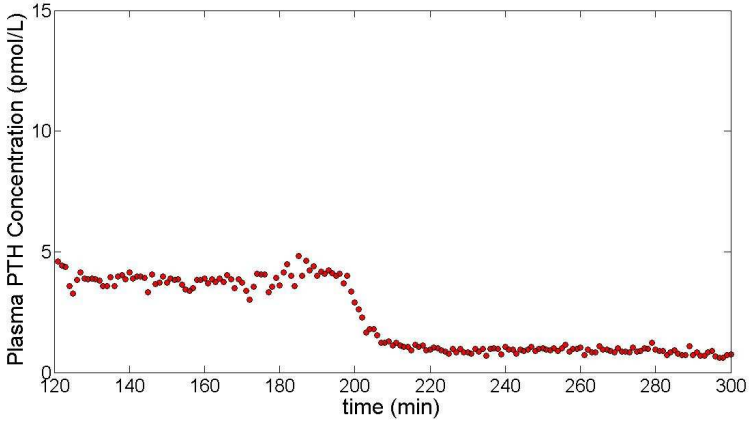

(d) PTH response for induced hypercalcemia.

Figure 3.2. An example of rapidly induced calcemic clamp test [20].

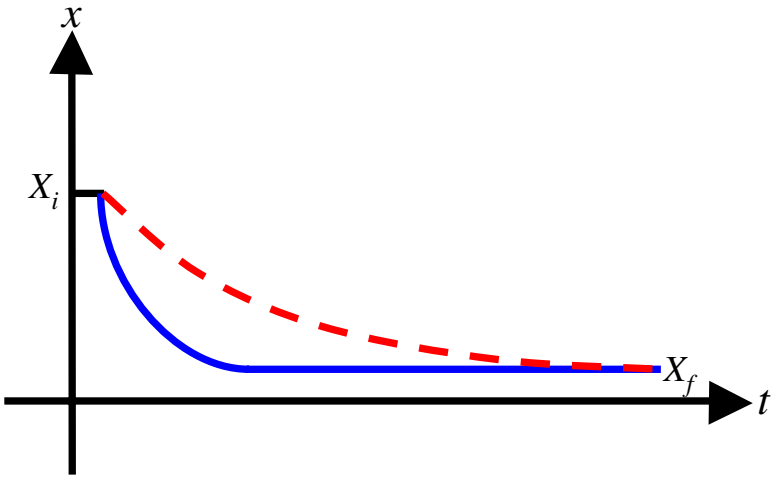

(a) Typical time profiles of plasma Ca^{++} concentrations, x, during induced hypocalcemic clamp tests. The dashed profile represents a slower decrease and the solid profile represents a faster decrease from initial steady-state X_i to a final steady-state X_f.

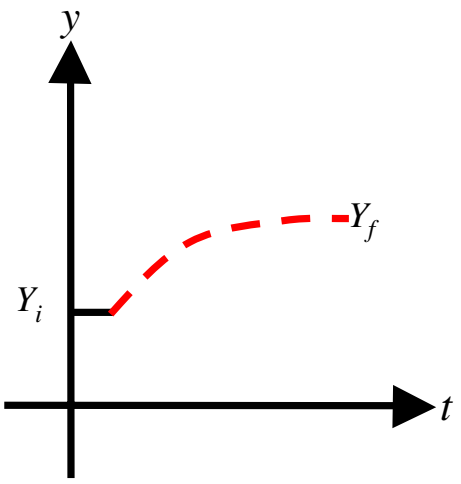

(b) A typical PTH response, y, to slow induction of hypocalcemia.

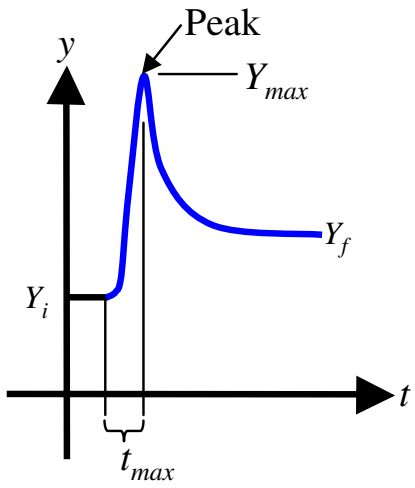

(c) A typical PTH response, y, to rapid induction of hypocalcemia. Note the conspicuous peak.

Figure 3.3. An illustration of typical results in induced hypocalcemic clamp tests.

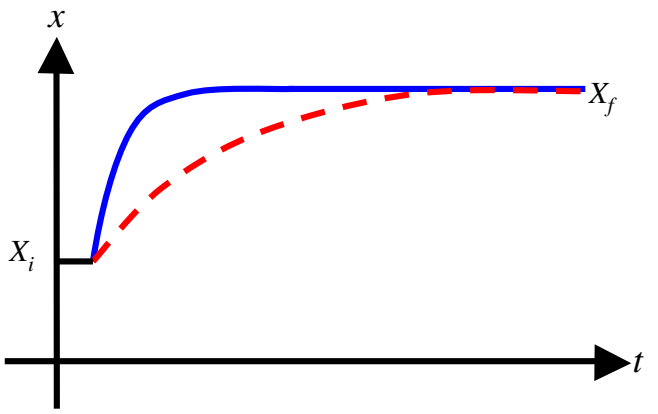

(a) Typical time profiles of plasma Ca^{++} concentrations, x, during induced hypercalcemic clamp tests. The dashed profile represents a slow increase and the solid profile represents a rapid increase from initial steady-state X_i to a final steady-state X_f.

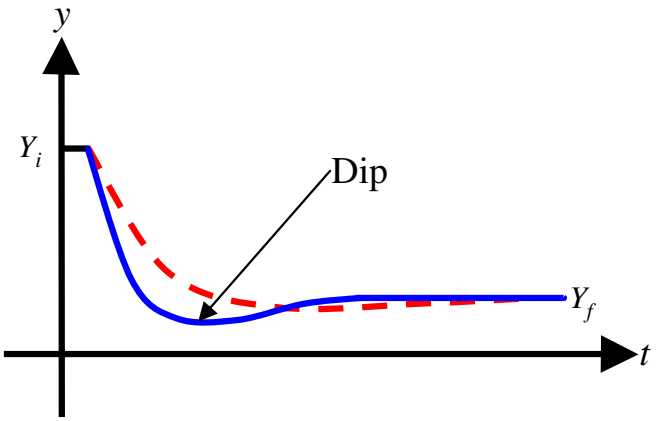

(b) A typical PTH response, y, to a slow induction of hypercalcemia represented by the dashed line and a rapid induction of hypercalcemia by represented by the solid line. Note the inconspicuous dip in PTH response for the rapid induction of hypercalcemia.

Figure 3.4. An illustration of typical results of induced hypercalcemic clamp tests.

glands (PTG pool) and the other in plasma (plasma pool), as shown in Figure 3.5. In

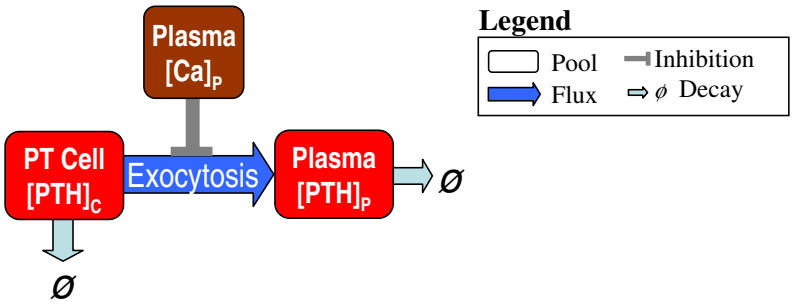

Figure 3.5. The Ca-PTH axis isolated from the qualitative model of calcium homeostasis shown in Figure 2.7.

response to an acute decrease (time-scale of minutes) in plasma Ca^{++} concentration, signaling pathways involving calcium sensors on the parathyroid chief cell stimulate exocytosis of the PTH stored in the vesicles of the cells. Similarly, they inhibit exocytosis of the PTH in response to a rise in the plasma Ca^{++} concentration. The PTH response occurs in time-scale of minutes [20]. Since we are considering the response of PTH to acute changes in plasma Ca^{++} concentration, we can assume the bio-synthesis rate of PTH to remain constant because the regulation of PTH bio-synthesis in response to changes in the plasma Ca^{++} concentration occurs in the times-scale of hours to days [1, 14, 18].

Using mass balance and assuming that we model average dynamics of n active chief cells in the parathyroid glands, the rate of change of PTH in the PTG pool is given by

$$\dot{x_1}(t) = \underbrace{k}_{PTH\ production} - \underbrace{\lambda_{\mathrm{Ca}}(t)x_1(t)}_{\text{Secretion to plasma}} - \underbrace{\lambda_1 x_1(t)}_{\text{Decay}}, \tag{3.1}$$

where $x_1(t)$ denotes the total amount of PTH in the PTG pool, k denotes the constant production rate of PTH in the PTG pool, $\lambda_{Ca}(t)$ denotes the secretion rate function which depends on plasma Ca^{++} concentration, and λ_1 denotes the decay rate constant of PTH

inside the parathyroid cells. We use the four-parameter reverse-sigmoidal relationship [33] to relate $\lambda_{Ca}(t)$ and plasma Ca^{++} concentration

$$\lambda_{\mathrm{Ca}}(t) = \frac{A - B}{1 + \left(\frac{Ca(t)}{S}\right)^m} + B, \tag{3.2}$$

where A and B denote maximal and minimal values of the secretion rate constant, $Ca(t)$ denotes plasma Ca^{++} concentration, and S is the value of $Ca(t)$ when $\lambda_{\mathrm{Ca}} = \frac{A+B}{2}$, and m gives the slope of the curve at S, respectively. These characteristic features of the reverse sigmoid relationship are depicted in Figure 3.6. EM Brown originally used this relationship

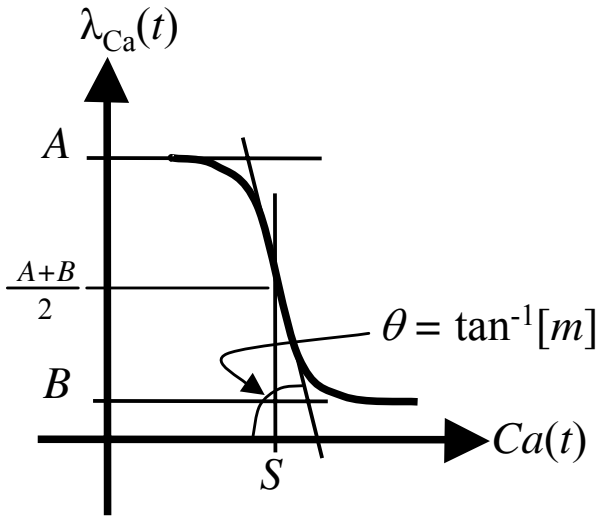

Figure 3.6. The reverse sigmoid curve.

[33] to relate PTH secretion rate and plasma Ca^{++} concentration. Note that we have used the relationship to relate PTH secretion function ($\lambda_{Ca}(t)$) to plasma Ca^{++} concentration and not PTH secretion (λ_{Ca}) to plasma Ca^{++} concentration. The rate of change of PTH in the plasma pool is given by a mass balance relation

$$\dot{x_2}(t) = \underbrace{\lambda_{\mathrm{Ca}}(t)x_1(t)}_{\text{Secretion from parathyroid glands to plasma}} - \underbrace{\lambda_2 x_2(t)}_{\text{Clearance}}, \tag{3.3}$$

where $x_2(t)$ denotes the amount of PTH in the plasma pool and λ_2 denotes the biological clearance rate constant for PTH in circulation. Writing Equations (3.1) and (3.3) in a matrix form

$$\begin{pmatrix} \dot{x_1} \\ \dot{x_2} \end{pmatrix} = \begin{pmatrix} -(\lambda_{\mathrm{Ca}}(t) + \lambda_1) & 0 \\ \lambda_{\mathrm{Ca}}(t) & \lambda_2 \end{pmatrix} \begin{pmatrix} x_1 \\ x_2 \end{pmatrix} + \begin{pmatrix} k & 0 \\ 0 & 0 \end{pmatrix} \begin{pmatrix} 1 \\ 0 \end{pmatrix}, \tag{3.4}$$

we observe that the two equations form a hierarchy of differential equations. We can solve the first equation, which has a constant forcing function reflecting the assumption of constant rate of PTH production at fast time-scale, to compute $x_1(t)$ and then substitute it into the second equation to solve for $x_2(t)$.

Note that λ_{Ca} is a function of time. Thus the dynamical system (3.4) is an LTV system. The solution of the system is given by

$$\begin{aligned} x_1(t) =& \phi_1(t,t_0)x_{10} + k\int_{t_0}^{t} \phi_1(t,\sigma)d\sigma \\ x_2(t) =& \phi_2(t,t_0)x_{20} + \int_{t_0}^{t} \phi_2(t,\sigma)\lambda_{\mathrm{Ca}}(\sigma)x_1(\sigma)d\sigma \end{aligned} \qquad t \geq t_0,\ x_1(t_0) = x_{10},\ x_2(t_0) = x_{20}, \tag{3.5}$$

where, $\phi_1(t,t_0)$, $\phi_2(t,t_0)$, $\phi_1(t,\sigma)$, and $\phi_2(t,\sigma)$ are transition scalars given by

$$\begin{aligned} \phi_1(t,t_0) =& e^{-\int_{t_0}^{t}(\lambda_{\mathrm{Ca}}(\sigma)+\lambda_1)d\sigma} = e^{-\int_{t_0}^{t}\left(\frac{A-B}{1+\left(\frac{Ca(\sigma)}{S}\right)^m}+\lambda_1\right)d\sigma} \\ \phi_2(t,t_0) =& e^{-\int_{t_0}^{t}\lambda_2 d\sigma} \\ \phi_1(t,\sigma) =& e^{-\int_{\sigma}^{t}(\lambda_{\mathrm{Ca}}(\tau)+\lambda_1)d\tau} = e^{-\int_{\sigma}^{t}\left(\frac{A-B}{1+\left(\frac{Ca(\tau)}{S}\right)^m}+\lambda_1\right)d\tau} \\ \phi_2(t,\sigma) =& e^{-\int_{\sigma}^{t}\lambda_2 d\tau}. \end{aligned}$$

We have used $Ca(t) = c_1 + c_2e^{-\lambda t}$ and $Ca(t) = c_3 - c_4e^{-\lambda t}$ to approximate calcium-time profiles during hypo- and hyper-calcemic clamp tests [see Figure 3.8(a) and Figure 3.9(a)].

Unfortunately, the solution (3.5) is analytically intractable because the integral terms on the right-hand side cannot be solved in a closed form. One way to simplify the analysis is to assume a step-change in calcium [19], which renders $\lambda_{Ca}(t)$ a constant and thus the system (3.4) becomes an LTI. Using $\lambda_{Ca}(t) = \lambda_{Ca}$, and $t_0 = 0$, we have

$$\begin{aligned}
\phi_1(t, t_0) =& e^{-(\lambda_{\mathrm{Ca}}+\lambda_1)\int_{t_0}^{t} d\sigma} = e^{-(\lambda_{\mathrm{Ca}}+\lambda_1)t} \\
\phi_2(t, t_0) =& e^{-\lambda_2 \int_{t_0}^{t} d\sigma} = e^{-\lambda_2 t} \\
\phi_1(t, \sigma) =& e^{-(\lambda_{\mathrm{Ca}}+\lambda_1)\int_{\sigma}^{t} d\tau} = e^{-(\lambda_{\mathrm{Ca}}+\lambda_1)(t-\sigma)} \\
\phi_2(t, \sigma) =& e^{-\lambda_2 \int_{\sigma}^{t} d\tau} = e^{-\lambda_2 (t-\sigma)}.
\end{aligned}$$

So, the solution is given by

$$\begin{aligned}
x_1(t) =& \frac{k}{\lambda_{\mathrm{Ca}} + \lambda_1} + \left(x_{10} - \frac{k}{\lambda_{\mathrm{Ca}} + \lambda_1} \right) e^{-(\lambda_{\mathrm{Ca}}+\lambda_1)t} \\
x_2(t) =& \frac{\lambda_{Ca} k}{(\lambda_{\mathrm{Ca}} + \lambda_1)\, \lambda_2} \\
&+ \left(x_{20} - \frac{\lambda_{Ca} k}{(\lambda_{\mathrm{Ca}} + \lambda_1)\, \lambda_2} + \frac{\lambda_{Ca} x_{10}}{(\lambda_{\mathrm{Ca}} + \lambda_1 - \lambda_2)} - \frac{\lambda_{Ca} k}{(\lambda_{\mathrm{Ca}} + \lambda_1)\, (\lambda_{\mathrm{Ca}} + \lambda_1 - \lambda_2)} \right) e^{-\lambda_2 t} \\
&+ \left(\frac{\lambda_{Ca} k}{(\lambda_{\mathrm{Ca}} + \lambda_1)\, (\lambda_{\mathrm{Ca}} + \lambda_1 - \lambda_2)} - \frac{\lambda_{\mathrm{Ca}} x_{10}}{(\lambda_{\mathrm{Ca}} + \lambda_1 - \lambda_2)} \right) e^{-(\lambda_{\mathrm{Ca}}+\lambda_1)t}.
\end{aligned}$$

In practice, Ca^{++} concentration changes at a much slower rate than a step. So the step-change assumption in plasma Ca^{++} concentration is not valid. Moreover, plasma PTH response depends on the rate of change of plasma Ca^{++} concentration [38, 43]. Thus a model has to be able to capture the expected time-varying nature of the system (3.4). Next we present our computational approach for parameterizing the system equations.

3.3.1 Model parametrization

We start by deriving parameter constraints of the system (3.1)-(3.3) at steady-state. We then use both known data and a guided iterative procedure to match clinical tests. In the following subsections we describe the model parametrization steps.

3.3.1.1 Deriving parameter constraints at steady-state

At steady-state, (3.1) becomes

$$k = \left[\frac{A-B}{1+\left(\frac{Ca_{SS}}{S}\right)^m} + B\right] x_{1,SS} + \lambda_1 x_{1,SS}, \tag{3.6}$$

where $x_{1,\mathrm{SS}}$ and Ca_{SS} denote steady-state values of PTH in the PTG pool and plasma Ca^{++} concentration in plasma, respectively. Similarly, (3.3) becomes

$$\left[\frac{A-B}{1+\left(\frac{Ca_{SS}}{S}\right)^m} + B\right] x_{1,SS} = \lambda_2 x_{2,\mathrm{SS}}, \tag{3.7}$$

where $x_{2,\mathrm{SS}}$ denotes steady-state values of PTH concentration in plasma. From (3.6) and (3.7) we have

$$k = \lambda_2 x_{2,\mathrm{SS}} + \lambda_1 x_{1,\mathrm{SS}}. \tag{3.8}$$

Considering normal steady-state[1] values of a healthy individual, 3.8 becomes

$$k = \lambda_2 x_{2,\mathrm{SS,N}} + \lambda_1 x_{1,\mathrm{SS,N}}, \tag{3.9}$$

where $x_{1,\mathrm{SS,N}}$ and $x_{2,\mathrm{SS,N}}$ are steady-state values of PTH in the PTG pool and PTH in plasma of a healthy individual, respectively. Since the steady-state PTH secretion rate in response to acute changes in plasma Ca^{++} has maximum and minimum saturation values [33], we assume that there is a maximum or a minimum saturation steady-state value that plasma PTH concentration can attain as well. At extreme values, (3.8) becomes

$$k = \lambda_2 x_{2,\mathrm{SS,Min}} + \lambda_1 x_{1,\mathrm{SS,Max}}, \tag{3.10}$$

[1]By normal steady-state we mean the average concentrations of either plasma Ca^{++} or PTH when an individual is not under clamp test.

and

$$k = \lambda_2 x_{2,\mathrm{SS,Max}} + \lambda_1 x_{1,\mathrm{SS,Min}}, \tag{3.11}$$

where $x_{1,\mathrm{SS,Max}}$ and $x_{1,\mathrm{SS,Min}}$ denote maximum and minimum steady-state values of PTH in the PTG pool, respectively, and $x_{2,\mathrm{SS,Min}}$ and $x_{2,\mathrm{SS,Max}}$ denote minimum and maximum steady-state values of PTH in the plasma pool, respectively. Evaluating (3.7) at upper and lower plasma Ca^{++} levels we have

$$\lim_{Ca\to 0} A x_{1,\mathrm{SS,Min}} = \lambda_2 x_{2,\mathrm{SS,Max}} \Longrightarrow A = \frac{\lambda_2 x_{2,\mathrm{SS,Max}}}{x_{1,\mathrm{SS,Min}}}, \tag{3.12}$$

$$\lim_{Ca\to \infty} A x_{1,\mathrm{SS,Max}} = \lambda_2 x_{2,\mathrm{SS,Min}} \Longrightarrow B = \frac{\lambda_2 x_{2,SS,Min}}{x_{1,SS,Max}}. \tag{3.13}$$

Finally, the set point S can be isolated from (3.2) as follows

$$S = \exp\left[\log\left(Ca_{\mathrm{SS}}\right) - \frac{1}{m}\log\left\{\left(\frac{A-B}{\frac{\lambda_2 x_{2,\mathrm{SS}}}{x_{1,\mathrm{SS}}} - B}\right) - 1\right\}\right]. \tag{3.14}$$

Relevant steady-state data is listed in Table 3.1 obtained from [20]. Since our model is based

Variables	Concentration	Units
$x_{2,\mathrm{SS,N}}$	2.41	pmolL^{-1}
$x_{2,\mathrm{SS,Max}}$	5.20	pmolL^{-1}
$x_{2,\mathrm{SS,Min}}$	0.96	pmolL^{-1}
$Ca_{\mathrm{SS,N}}$	1.23	mmolL^{-1}

Table 3.1. Average steady-state plasma PTH ($x_{2,SS}$) and Ca^{++} concentrations from 7 healthy individuals obtained from Figure 3.2 [20].

on mass balance, the available data in concentration units (pmolL^{-1}) have been multiplied

by average adult plasma volume, $\approx$ 2.75 L [44], to convert into pmols and listed in Table 3.2.

Variables	Amount	Units
$x_{2,\mathrm{SS,N}}$	6.63	pmol
$x_{2,\mathrm{SS,Max}}$	14.39	pmol
$x_{2,\mathrm{SS,Min}}$	2.65	pmol

Table 3.2. Data from Table 3.1 converted into pmols.

There are 10 unknowns, $k,\ \lambda_1,\ \lambda_2,\ x_{1,\mathrm{SS,N}},\ x_{1,\mathrm{SS,Max}},\ x_{1,\mathrm{SS,Min}},\ A,\ B,\ S$, and m, in the 6 equations (3.9)-(3.14). If we know the values of $\lambda_1,\ \lambda_2,\ x_{1,\mathrm{SS,N}}$, and m we can get a closed form solution for the rest of the unknowns. These four unknowns can have infinite number of possible values. Our aim is to find values that make appropriate biological sense. The resulting numerical solution of (3.1)-(3.3) should also match well with the clinical data (presented in Section 3.2). Next, we present some information that we utilized to define a reasonable starting values of these four unknowns.

3.3.1.2 Estimating starting values of $\lambda_1,\ \lambda_2$, $x_{1,\mathrm{SS,N}}$, and m

1. The half-life of PTH in circulation, $\tau_2 = \frac{\ln(2)}{\lambda_2}$, has been reported to vary from 2 to 15 minutes in [19], 2.04-2.93 minutes in [20], and 2.5 in [37]. The later also states that these values represent upper estimates, as any continued PTH release above the post infusion baseline during the decay measurements would slightly prolong the calculated half-life. Hence, we assume plasma PTH disappearance half life in a healthy adult to be less than 15 minutes. As a starting value we used τ_2=2.5 minutes. So, $\lambda_2 = \frac{\ln(2)}{\tau_2}$.

2. We assume that the half-life of PTH in the parathyroid cell, $\tau_1 = \frac{\ln(2)}{\lambda_1}$, is much greater than τ_2, since there is no clearance by kidney or liver while the PTH is still in the chief cell. As a starting value we have used τ_1= 30 minutes. So, $\lambda_1 = \frac{\ln(2)}{\tau_1}$.

3. We assume that $x_{1,\mathrm{SS,N}} >> x_{2,\mathrm{SS,N}}$ when there is no acute disturbance in the plasma calcium level. Clinical data in [20, 38] suggests that a sustained high PTH secretion rate is possible for hours during sustained hypocalcemia. Since the rate of biosynthesis doesn't vary substantially in that time scale [1, 14, 19], this sustained secretion of PTH at a higher rate is only possible if there is a very large storage of PTH in the vesicles of the PTG pool. Thus, we have used $x_{1,\mathrm{SS,N}} = 10 \times x_{2,\mathrm{SS,N}}$ as the starting value.

4. The parameter m controls the sensitivity of $\lambda_{Ca}(t)$ with respect to the plasma Ca^{++} concentration. We have used $m = 100$ as a starting point, assuming a very high sensitivity consistent with observations from clinical data [33, 42].

At this point we only know the starting guess values of the four unknowns $\lambda_1,\ \lambda_2$, $x_{1,\mathrm{SS,N}}$, and m which we will use for the guided iteration. The next step is to calculate k, $x_{1,\mathrm{SS,Max}}$, $x_{1,\mathrm{SS,Min}}$, $A,\ B$, and S.

3.3.1.3 Calculating k, $x_{1,\mathrm{SS,Max}}$, $x_{1,\mathrm{SS,Min}}$, $A,\ B$, and S

We use the six equations (3.9)-(3.14) to calculate k, $x_{1,\mathrm{SS,Max}}$, $x_{1,\mathrm{SS,Min}}$, $A,\ B$, and S respectively:n

$$
\begin{aligned}
k &= \lambda_2 x_{2,\mathrm{SS,N}} + \lambda_1 x_{1,\mathrm{SS,N}}, \\
x_{1,\mathrm{SS,Max}} &= \frac{k - \lambda_2 x_{2,\mathrm{SS,Min}}}{\lambda_1}, \\
x_{1,\mathrm{SS,Min}} &= \frac{k - \lambda_2 x_{2,\mathrm{SS,Max}}}{\lambda_1}, \\
A &= \frac{\lambda_2 x_{2,\mathrm{SS,Max}}}{x_{1,\mathrm{SS,Min}}}, \\
B &= \frac{\lambda_2 x_{2,SS,Min}}{x_{1,SS,Max}}, \text{ and} \\
S &= \exp\left[\log\left(Ca_{\mathrm{SS}}\right) - \frac{1}{m}\log\left\{\left(\frac{A-B}{\frac{\lambda_2 x_{2,\mathrm{SS}}}{x_{1,\mathrm{SS}}} - B}\right) - 1\right\}\right].
\end{aligned}
$$

At this point we have estimated the values of all the parameters k, λ_1, λ_2, A, B, S, and m for our model (3.1)-(3.3). The next step is to see if our model simulation can match clinical data of a hypocalcemic clamp test using these values. For this, we looked to match the features of the curve such as the peak value $Y_{\max}$, the time taken to reach this value $t_{\max}$, and the rate of exponential decrease of plasma PTH concentration from $Y_{\max}$ to the final steady-state Y_f as shown in Figure 3.3. The next step is to tune the values of the four parameters: λ_1, λ_2, $x_{1,\mathrm{SS,N}}$, and m from the starting values mentioned in Section 3.3.1.2 in an iterative fashion to get a better match. Some observations made during this tuning process were used as guidelines for tuning process as described in the following section.

3.3.1.4 Guidelines for tuning λ_1, λ_2, $x_{1,\mathrm{SS,N}}$, and m

1. Increasing τ_1 (or decreasing λ_1) increases $Y_{\max}$, decreases $t_{\max}$ and increases the rate of exponential decrease of PTH after peak in PTH response.

2. Increasing τ_2 (or decreasing λ_2) decreases $Y_{\max}$ and increases $t_{\max}$ and decreases the rate of exponential decrease of PTH after peak in PTH response.

3. Increasing $x_{1,\mathrm{SS,N}}$ decreases $Y_{\max}$ and increases $t_{\max}$ larger.

4. Increasing m increases $Y_{\max}$ and increases $t_{\max}$ larger.

The above guideline is diagrammatically represented in Figure 3.7. Using these guidelines we iteratively tune the values of λ_1, λ_2, $x_{1,\mathrm{SS,N}}$, and m until we achieve a good match with the hypocalcemic clamp test data.

This guided iterative process results in the parameter values listed in Table 3.3. The values of the remaining unknown parameters calculated from the steady-state relations (3.9)-(3.14) are listed in Table 3.4. Using these parameters, our simulation result (Figure 3.8(b)) matches very well with the plasma PTH response presented in Figure 3.2(b) for the calcium input as shown in Figure 3.2(a).

Action \ Result	Y_{max}	t_{max}	Rate of Exponential Decrease of PTH after Peak
τ_1 ↑	↑	↓	↑
τ_2 ↑	↓	↑	↓
$X_{1,SS,N}$ ↑	↓	↑	-
m ↑	↑	↑	-

Figure 3.7. The qualitative effects of tuning the parameters on PTH response for hypocalcemic clamp test simulation.

Parameters	Values	Units
τ_1	55.0000	min
λ_1	0.0126	min^{-1}
τ_2	1.8000	min
λ_2	0.3851	min^{-1}
$x_{1,SS,N}$	321.7500	pmol
m	170.0000	–

Table 3.3. Values of model parameters tuned to fit average induced hypocalcemic clamp test data obtained from 7 healthy individuals in Figure 3.8(b) [20].

Next, we used this model to predict the dynamics of hypercalcemic clamp test conducted on the same set of healthy subjects (Figure 3.2(d)). The same model, with the same set of parameters as in Table 3.3 successfully predicted observed clinical data as seen in Figure 3.9(b).

3.3.2 Guided iterative parametrization scheme

Listed below are the general steps used to parameterize our model:

1. Derive steady-state relations (3.9)-(3.14).

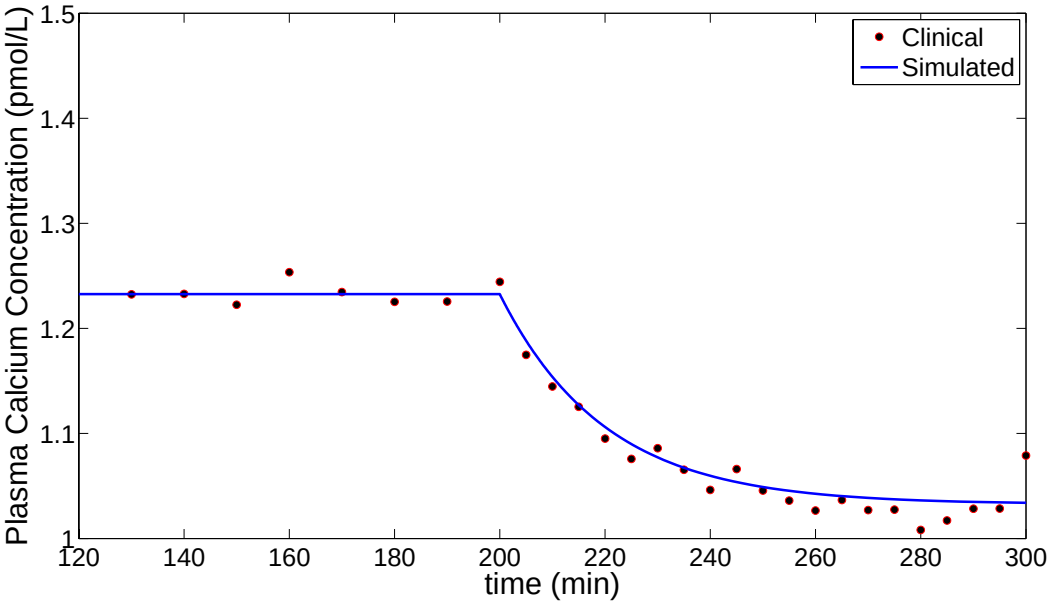

(a) Induced hypocalcemia (input).

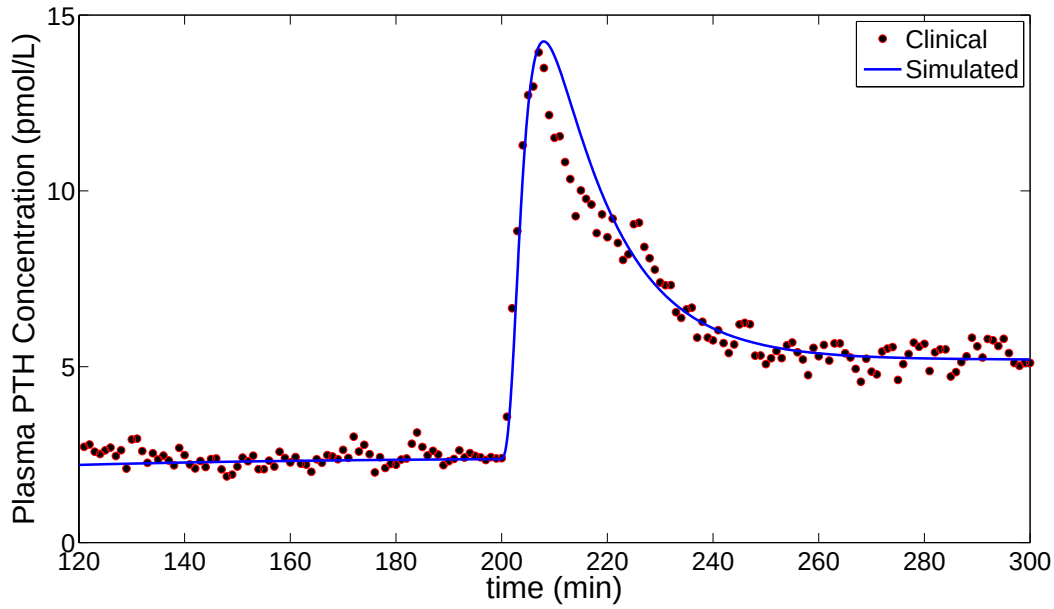

(b) PTH response for induced hypocalcemia (output).

Figure 3.8. Clinical (dots) vs. tuned-model simulation (solid lines) result of an induced hypocalcemic clamp test. Clinical data represents the average response of 7 healthy subjects [20].

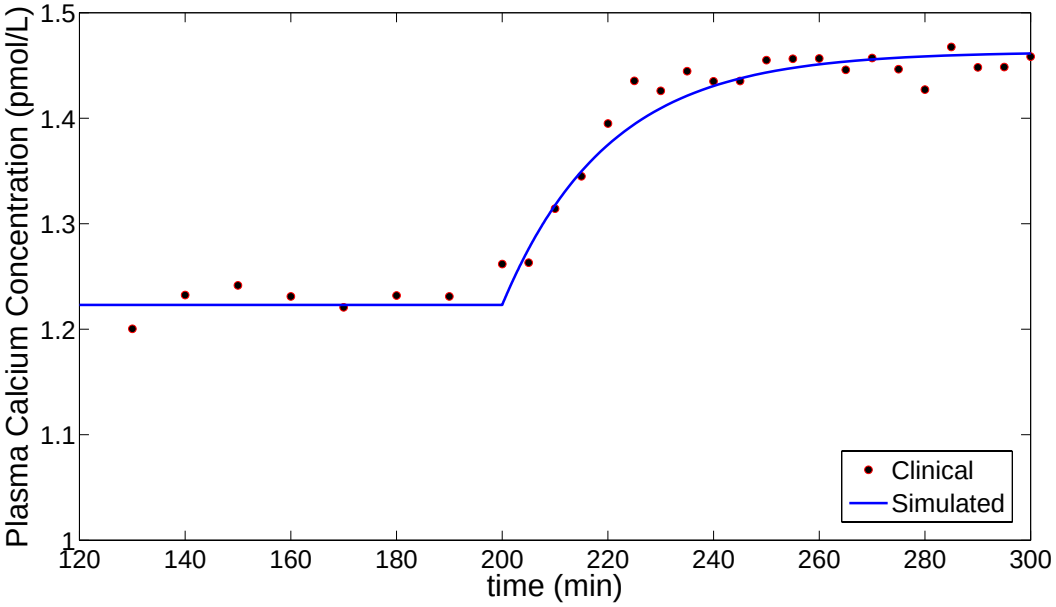

(a) Induced hypercalcemia (input).

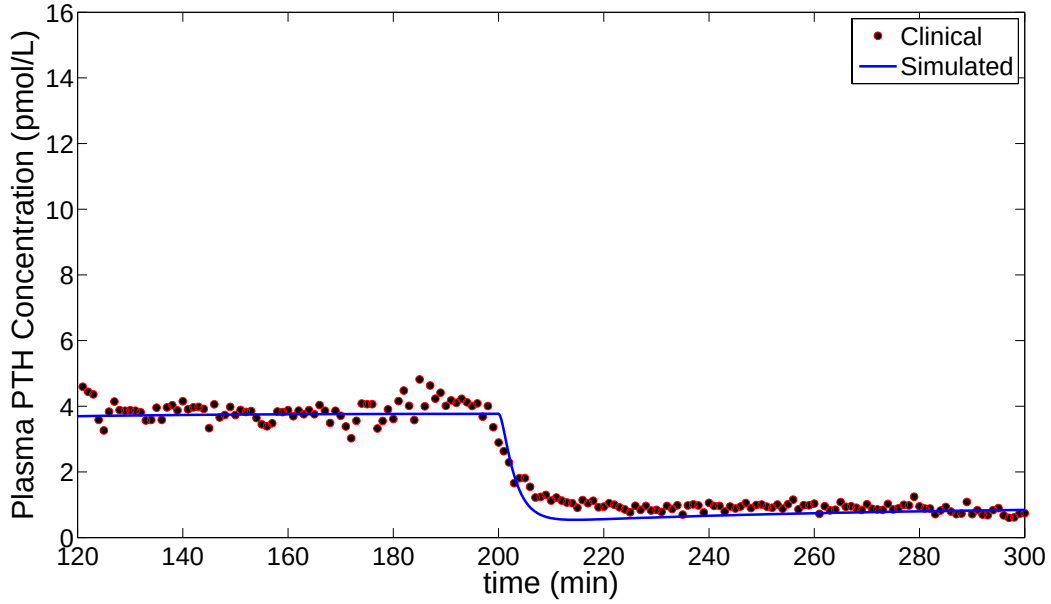

(b) PTH response for induced hypercalcemia (output).

Figure 3.9. Clinical (dots) vs. prediction by tuned-model (solid lines) of an induced hypercalcemic clamp test. Clinical data represents the average response of 7 healthy subjects [20].

Parameters	Values	Units
k	6.6102	pmol/min
$x_{1,\mathrm{SS,Max}}$	443.5062	pmol
$x_{1,\mathrm{SS,Min}}$	84.6236	pmol
A	0.0655	pmol/min
B	0.0023	pmol/min
S	1.2159	mmol/L

Table 3.4. Values of model parameters calculated using Table 3.3 and equations (3.9)-(3.14).

2. Estimate the starting values of λ_1, λ_2, $x_{1,\mathrm{SS,N}}$, and m based on the guidelines presented in the Subsection 3.3.1.2.

3. Calculate k, $x_{1,\mathrm{SS,Max}}$, $x_{1,\mathrm{SS,Min}}$, A, B, and S using (3.9)-(3.14), using the starting guess from step 2 and the available steady-state data for $x_{2,\mathrm{SS,N}}$, $x_{2,\mathrm{SS,Max}}$, $x_{2,\mathrm{SS,Min}}$, and $Ca_{\mathrm{SS,N}}$.

4. Use the values of k, λ_1, λ_2, A, B, S, and m obtained from steps 2 and 3 to produce the response of our model (3.1)-(3.3) to the input approximating data presented in Figure 3.8(a) numerically using a simulink model in matlab.

5. Compare the clinical data and model simulation [Figure 3.8(b)] with respect to various features of the curve such as $Y_{\max}$, $t_{\max}$ and the rate of exponential decrease of PTH after peak. If they don't match well , tune the value of one of the parameters λ_1, λ_2, $x_{1,\mathrm{SS,N}}$, and m based on the guidelines set forth in subsection 3.3.1.4 and go to step 3. Stop if a favorable match is achieved between them.

The final result obtained by following the guided iterative parametrization scheme as described above is presented in Figure 3.8(b).

To further test our model and the guided iterative parametrization scheme, we obtained proprietary data from the lead author of [20], Prof. Claus P Schmitt, Division of Pediatric

Nephrology, University of Heidelberg, Germany. These data describe the responses of 3 healthy individuals to hypo- and hyper-calcemic clamp test. From these data we found the steady-state values for $x_{2,\mathrm{SS,N}}$, $x_{2,\mathrm{SS,Max}}$, $x_{2,\mathrm{SS,Min}}$, and $Ca_{\mathrm{SS,N}}$ for these individuals which has been tabulated in Table 3.5. We followed the guided iterative parametrization scheme presented in Section 3.3.2. The final values of λ_1, λ_2, $x_{1,\mathrm{SS,N}}$, and m tuned to match the induced hypocalcemic clamp test data appear in Table 3.6. The calculated values of the unknown parameters in the steady-state Equations (3.9)-(3.14) are given in Table 3.7. The results of model parametrization and model prediction for these data from individual subjects are shown in Figures 3.10-3.15. Note that for the induced hypercalcemic clamp test for individual subjects (e.g., Figure 3.11), a portion of the transient data is missing. Unfortunately, this data could not be made available by Prof. Schmitt.

Subject	$x_{2,\mathrm{SS,N}}$ (pmolL^{-1})	$x_{2,\mathrm{SS,Min}}$ (pmolL^{-1})	$x_{2,\mathrm{SS,Max}}$ (pmolL^{-1})	$Ca_{\mathrm{SS,N}}$ (mmolL^{-1})
1	2.6767	0.4896	6.0320	1.2000
2	2.7527	0.5077	6.2027	1.2475
3	3.1044	0.7573	6.8011	1.2500

Table 3.5. Steady-state data of the individual subjects.

Subject	τ_1 (min)	λ_1 (min^{-1})	τ_2 (min)	λ_2 (min^{-1})	$x_{1,SS,N}$ (pmolL^{-1})	m
1	48.0	0.0144	1.43	0.4647	412.50	100
2	21.0	0.0330	0.70	0.9902	412.50	100
3	49.5	0.0140	1.10	0.6301	563.75	50

Table 3.6. Values of model parameters tuned to fit induced hypocalcemic clamp test data of the individual subjects.

Based on the successful predictive tests presented in this chapter we conclude that our two-pool, linear, time-varying model (3.1)-(3.3) provides a reasonable description of expected dynamics of the Ca-PTH axis. This is the first report of its kind to the best of our knowledge.

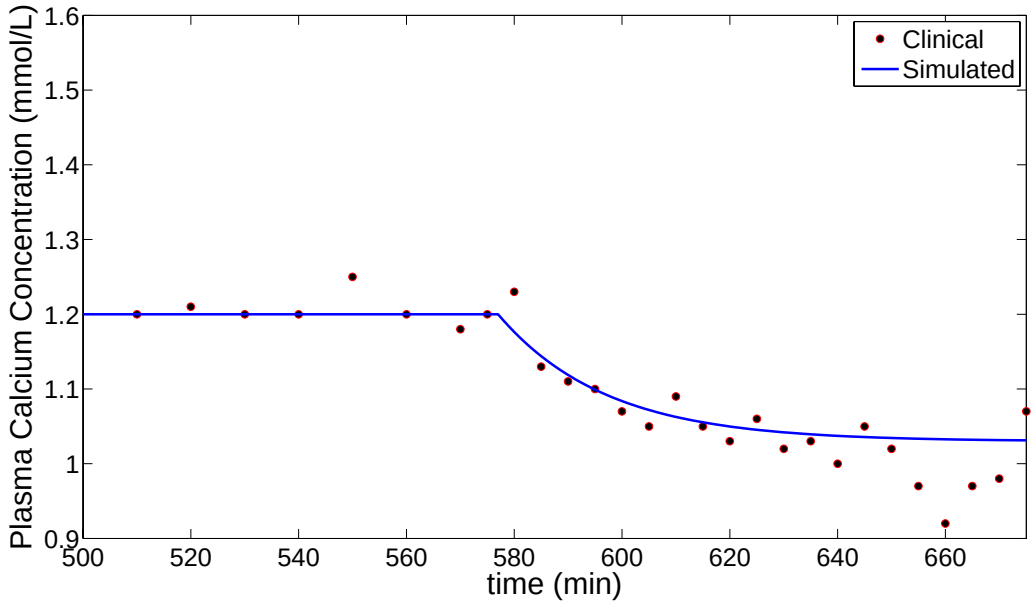

(a) Induced hypocalcemia (input).

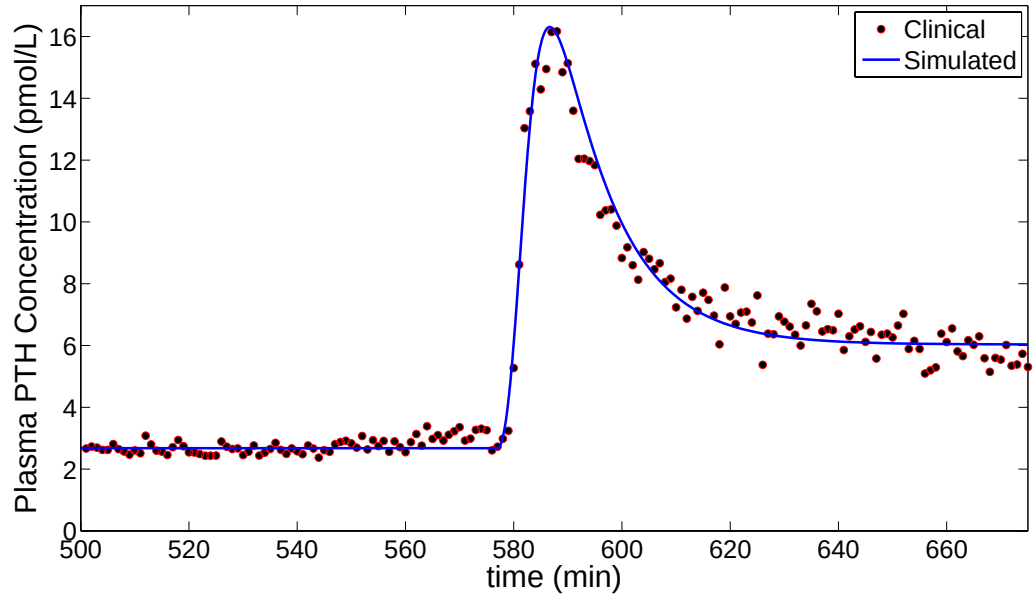

(b) PTH response for induced hypocalcemia (output).

Figure 3.10. Clinical (dots) vs. tuned-model simulation (solid line) of an induced hypocalcemic clamp test conducted on a healthy individual (Subject 1). Clinical data provided by the lead author of [20], Prof. Claus P Schmitt, Division of Pediatric Nephrology, University of Heidelberg, Germany.

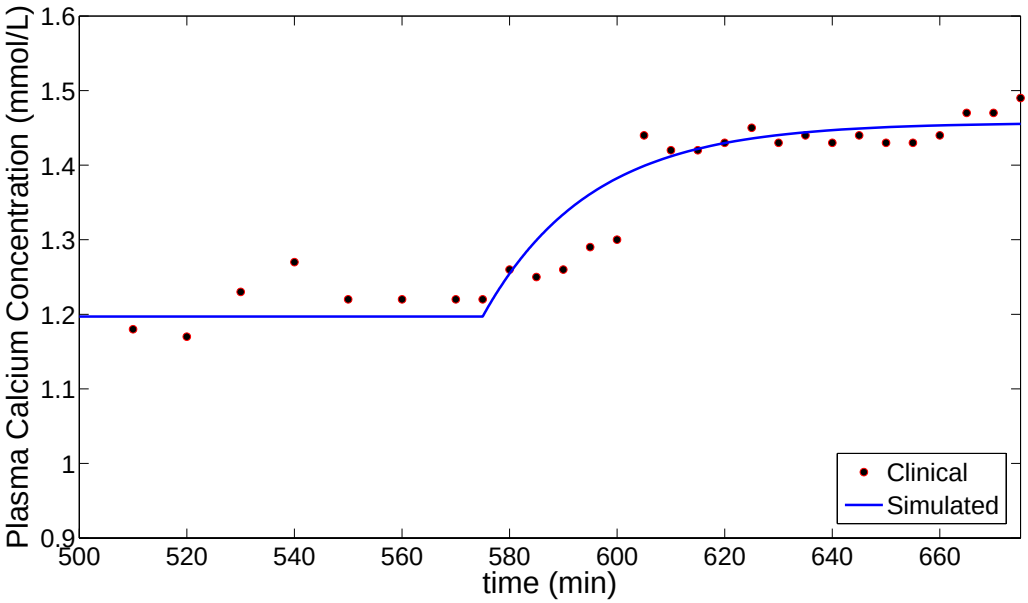

(a) Induced hypercalcemia (input).

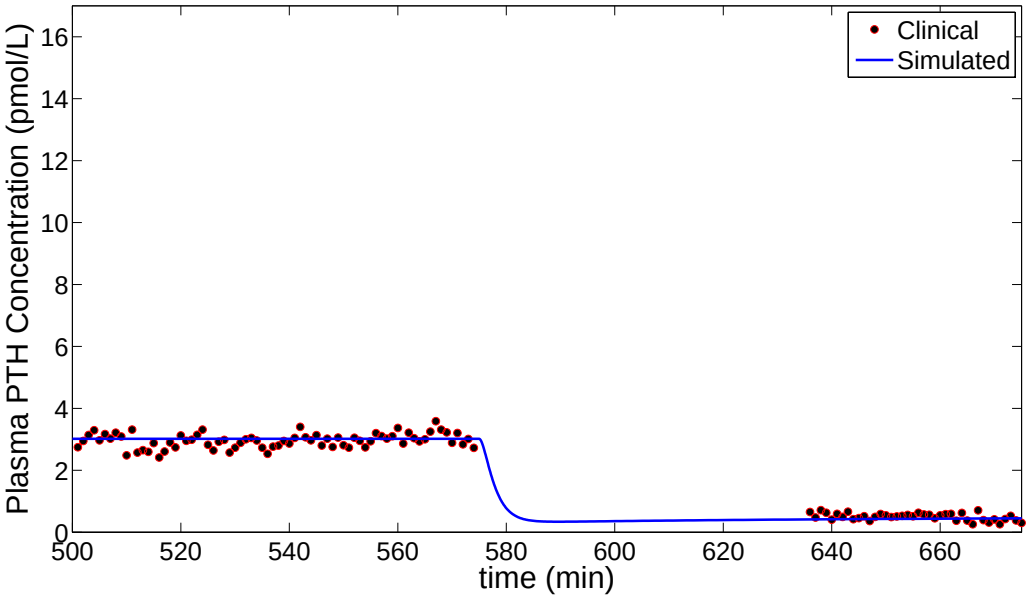

(b) PTH response for induced hypercalcemia (output).

Figure 3.11. Clinical (dots) vs. prediction by tuned-model (solid line) of an induced hypercalcemic clamp test conducted on a healthy individual (Subject 1). Clinical data provided by the lead author of [20], Prof. Claus P Schmitt, Division of Pediatric Nephrology, University of Heidelberg, Germany. Note: Prof. Schmitt could provide only the steady-state data but not the transient data for the PTH response.

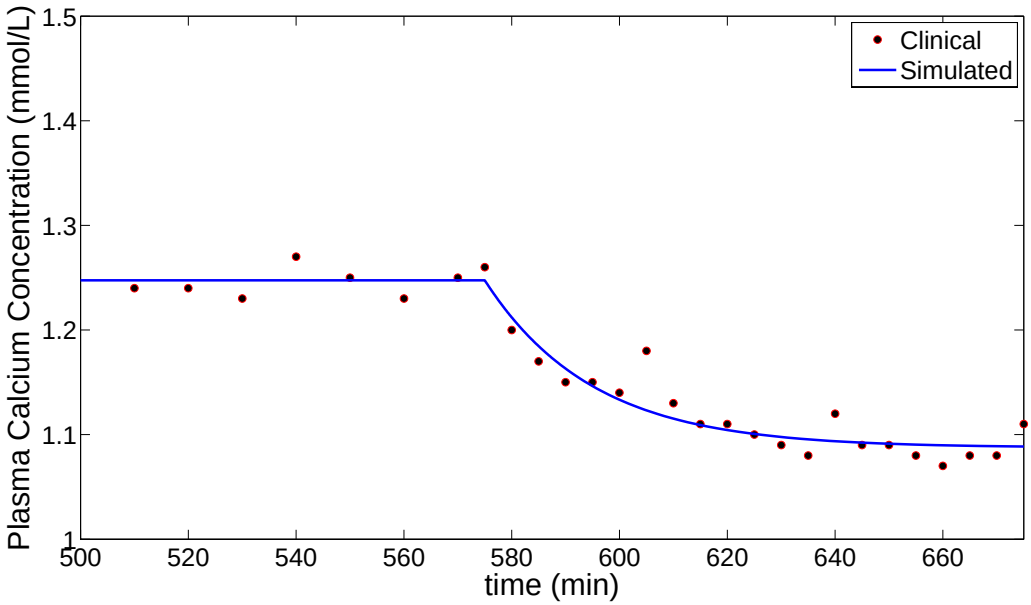

(a) Induced hypocalcemia (input).

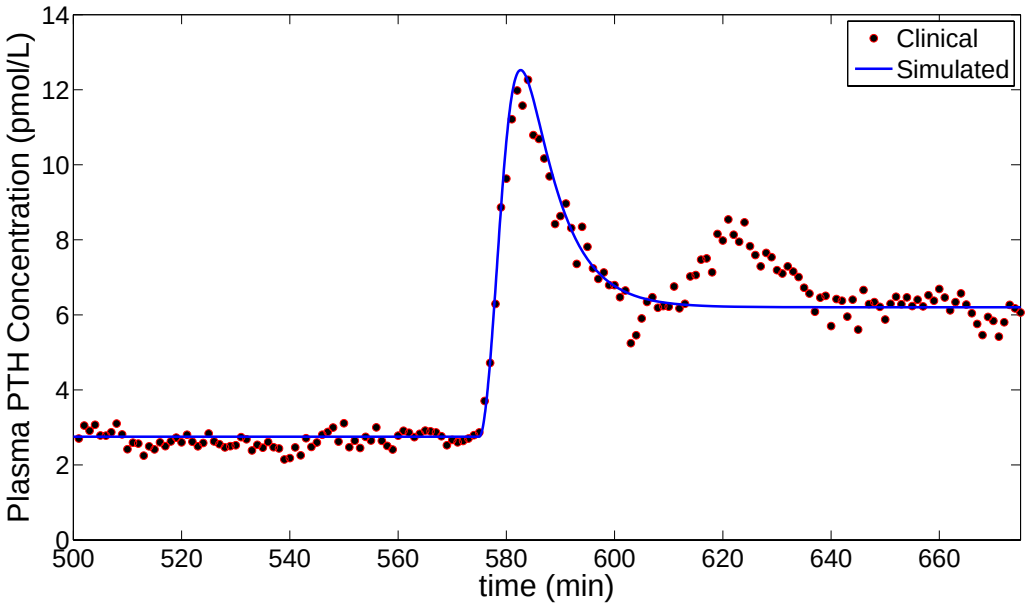

(b) PTH response for induced hypocalcemia (output).

Figure 3.12. Clinical (dots) vs. tuned model simulation (solid line) results of an induced hypocalcemic clamp test conducted on a healthy individual (Subject 2) provided by the lead author of [20], Prof. Claus P Schmitt, Division of Pediatric Nephrology, University of Heidelberg, Germany. Note the non-smooth nature of Ca^{++} which translates into non-smooth PTH response at >600 minutes. This prediction is based on the smooth (solid) Ca^{++} dynamics shown in (a). So such non-smooth behavior is not accounted for.

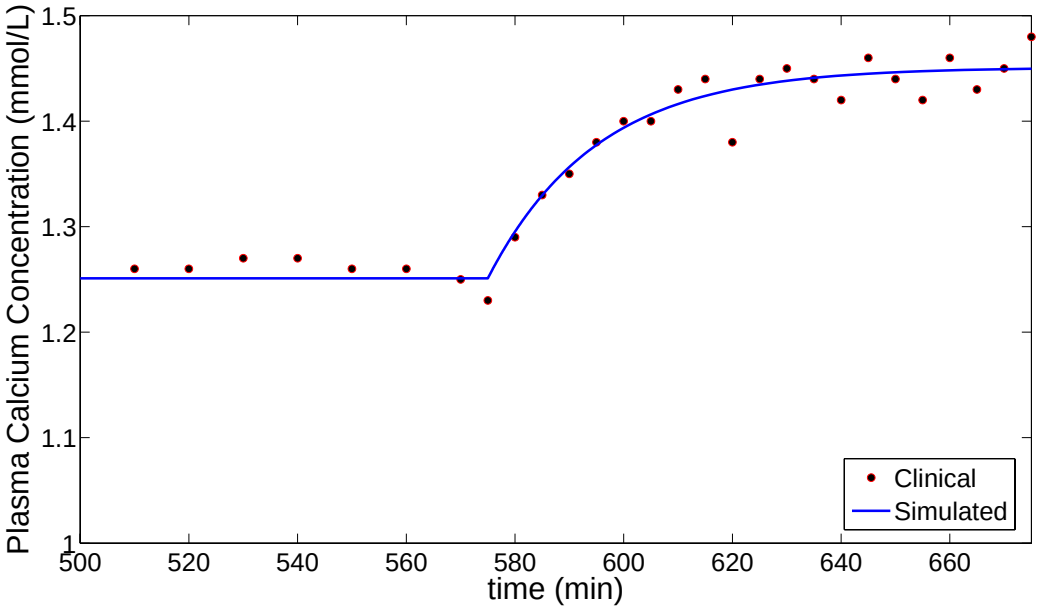

(a) Induced hypercalcemia (input).

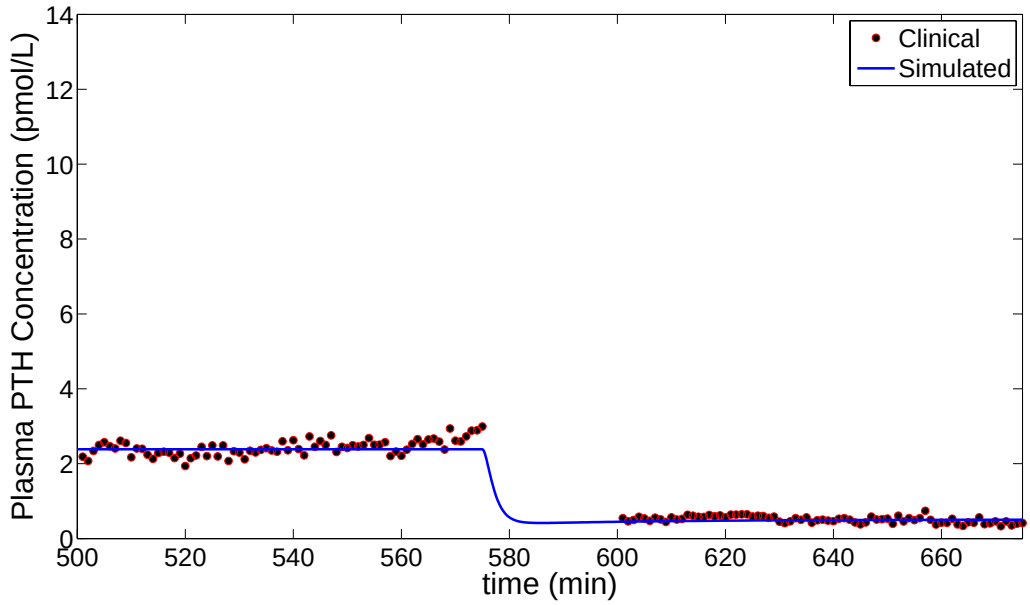

(b) PTH response for induced hypercalcemia (output).

Figure 3.13. Clinical (dots) vs. prediction by tuned-model (solid line) of an induced hypercalcemic clamp test conducted on a healthy individual (Subject 2). Clinical data provided by the lead author of [20], Prof. Claus P Schmitt, Division of Pediatric Nephrology, University of Heidelberg, Germany.

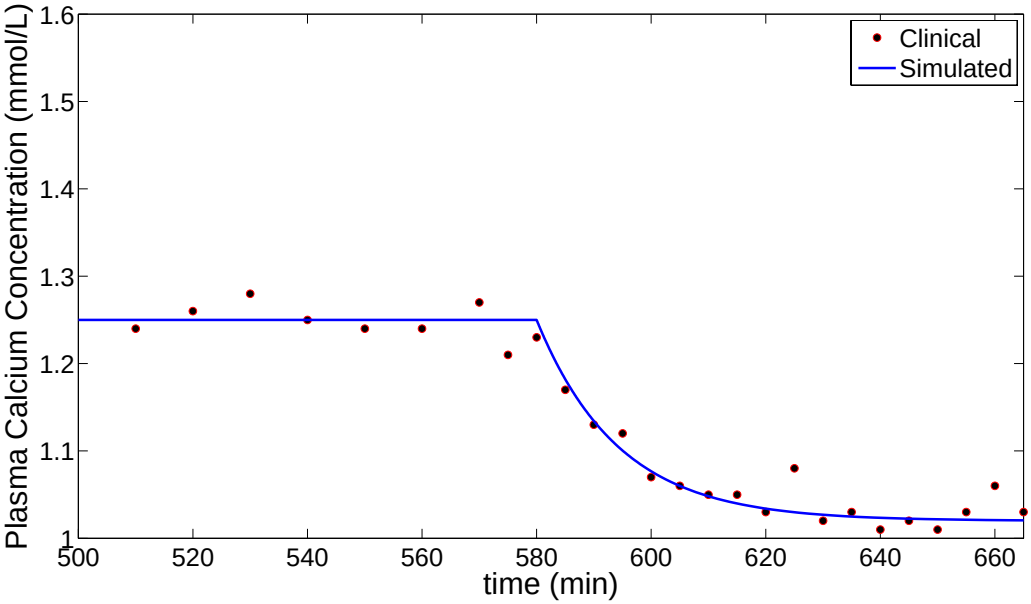

(a) Induced hypocalcemia (input).

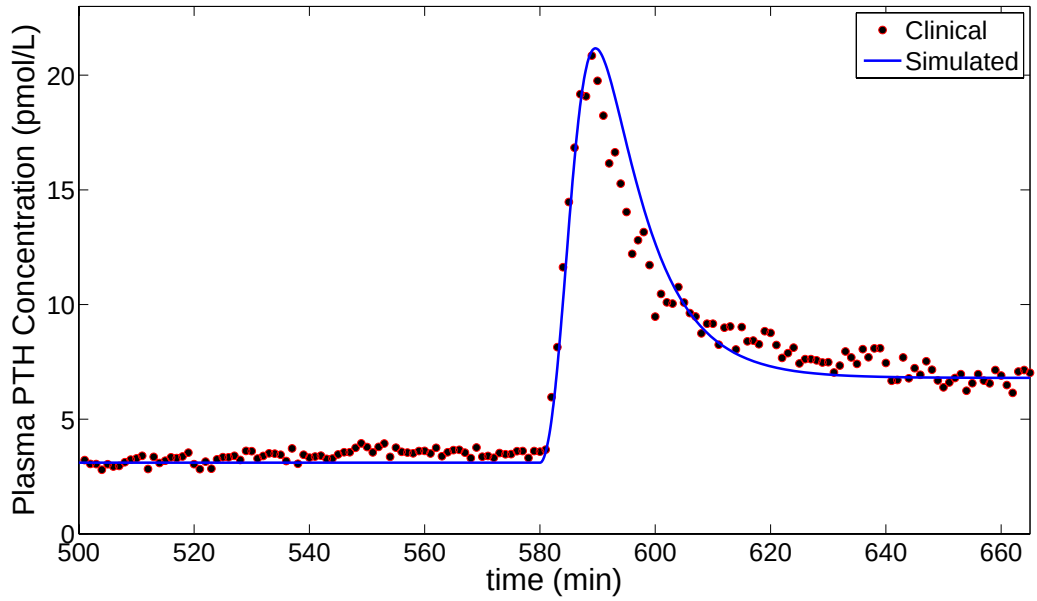

(b) PTH response for induced hypocalcemia (output).

Figure 3.14. Clinical (dots) vs. tuned-model simulation (solid line) of an induced hypocalcemic clamp test conducted on a healthy individual (Subject 3). Data provided by the lead author of [20], Prof. Claus P Schmitt, Division of Pediatric Nephrology, University of Heidelberg, Germany.

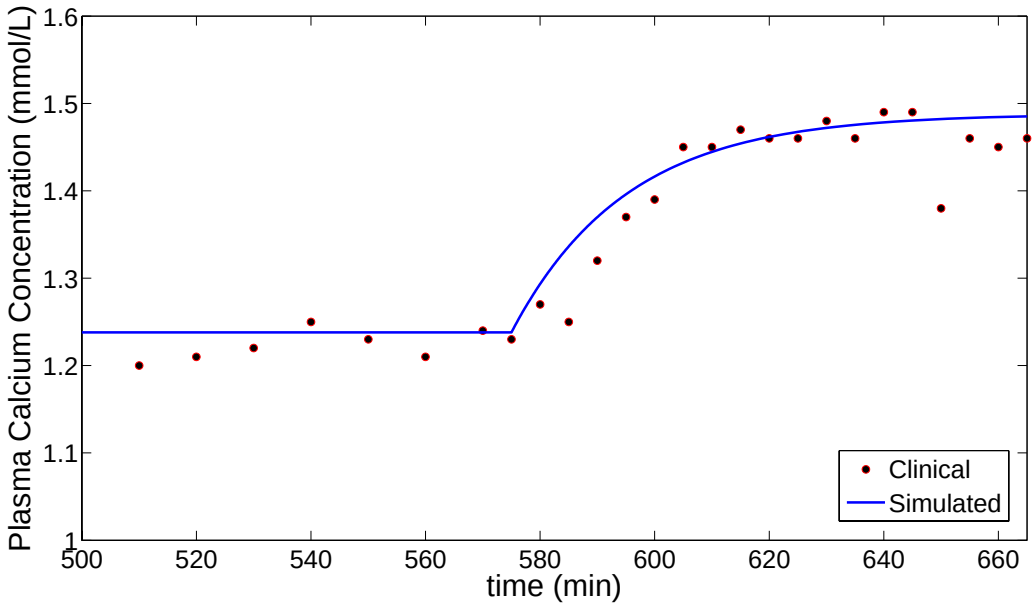

(a) Induced hypercalcemia (input).

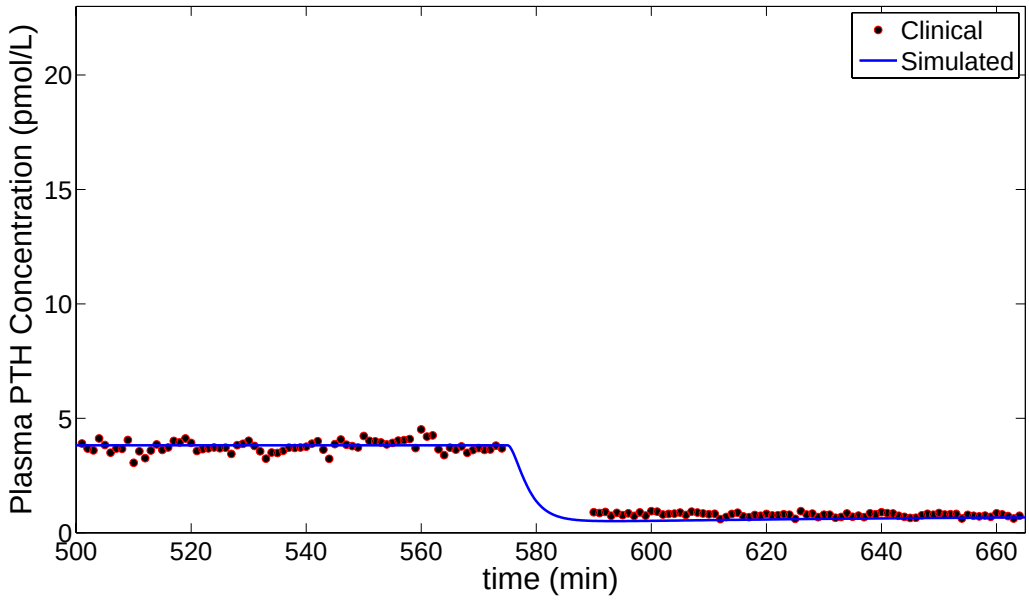

(b) PTH response for induced hypercalcemia (output).

Figure 3.15. Clinical (dots) vs. prediction by tuned-model (solid line) of an induced hypercalcemic clamp test conducted on a healthy individual (Subject 3). Clinical data provided by the lead author of [20], Prof. Claus P Schmitt, Division of Pediatric Nephrology, University of Heidelberg, Germany. Note: Prof. Schmitt could provide only the steady-state data but not the transient data for the PTH response.

Subjects	k	$x_{1,SS,Max}$	$x_{1,SS,Min}$	A	B	S
1	9.5247	614.3838	102.7813	0.0782	0.0011	1.1737
2	21.1112	597.7091	127.8721	0.1321	0.0023	1.2231
3	13.2737	854.2064	106.2867	0.1109	0.0015	1.1881
Units	$\text{pmolL}^{-1}\text{min}^{-1}$	pmolL^{-1}	pmolL^{-1}	min^{-1}	min^{-1}	mmolL^{-1}

Table 3.7. Values of model parameters for individual subjects calculated using Table 3.6 and equations (3.9)-(3.14).

The guided iterative method that relies on the available clinical data and biologically-driven assumptions provides a simple and an intuitive parametrization of our model. In the next chapter, we turn our focus to the calcium-PTH (Ca-PTH) reverse sigmoid curve.

CHAPTER 4

THE CA-PTH REVERSE SIGMOID CURVE

The reverse sigmoid curve describing steady-state Ca-PTH relationship has been suggested as a possible bio-tool for assessing health and disease states associated with calcium homeostasis [40, 41, 45, 46]. However, our analysis revealed that the accepted method implemented to quantify this curve has certain weaknesses. In this context, we present a new protocol to obtain a consistent Ca-PTH reverse sigmoid curve that is independent of the dynamics of the Ca-PTH axis and the induced calcemic clamp test procedure. We begin with a literature review.

4.1 Literature review

The reverse sigmoid relationship between plasma Ca^{++} and PTH concentrations in vivo was first reported in 1974 in Jersey cows from the plasma samples collected before, during and after parturition [47]. In 1978 Mayer, one of the co-authors of [47], and Hurst reported a reverse sigmoid relationship between plasma Ca^{++} concentration and PTH secretion rate [48]. Instead of measuring plasma PTH concentration, PTH secretion rate was measured directly by collecting PTH gland effluent blood samples from cows at regular intervals to measure the blood flow rate and the concentrations of PTH. The experiment was conducted over a period of 5 to 7 hours. Brown et al., also in 1978, studied the relationship of PTH release to Ca^{++} concentration in vitro [49]. The study was conducted on dispersed parathyroid cells of normal and abnormal parathyroid tissues from patients with adenoma or primary hyperplasia. Brown et al. published a series of similar studies conducted on the dispersed

parathyroid cells from patients with hyperparathyroidism [50], adenoma [51] and secondary hyperparathyroidism due to chronic renal failure [52]. In 1983, EM Brown, for the first time proposed the four parameter mathematical model [33] to describe the reverse sigmoidal relationship between parathyroid hormone release and Ca^{++} concentration in vitro observed in earlier data [49, 50, 51, 52]. This model was described by

$$y = \frac{A - B}{1 + \left(\frac{x}{S}\right)^m} + B \tag{4.1}$$

where y denotes PTH secretion rate, x denotes the Ca^{++} concentration, A denotes maximal PTH secretion rate, B denotes minimal PTH secretion rate, S denotes the value of x at which $y = \frac{A+B}{2}$, and m denotes the slope of the curve at S as shown in Figure 4.1.

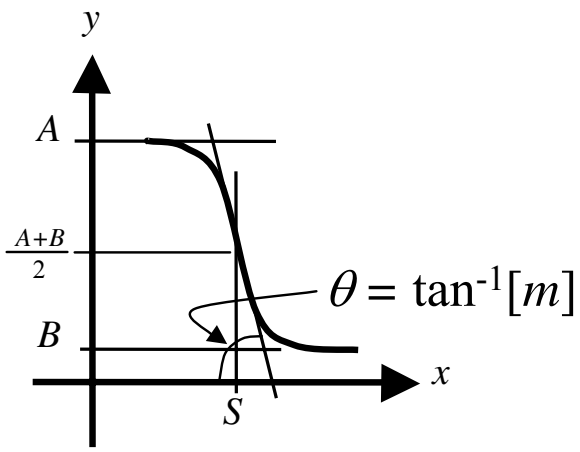

Figure 4.1. A reverse sigmoid curve.

Hysteresis in the relationship between the plasma Ca^{++} and PTH concentrations was reported in [39]. Hysteresis of PTH response to hypocalcemia in hemodialysis patients with bone disease was reported in [53]. In [42] it has been hypothesized that hysteresis in the relationship between plasma Ca^{++} concentration and PTH secretion in normal animals and humans and in hemodialysis patients results from a sensing of directional change or

acceleration or deceleration in the rate of change of the plasma Ca^{++} concentration by the parathyroid glands.

Numerous clinical studies utilized the reverse sigmoid curve to find possible correlation with normal and diseased calcium homeostasis. For example, studies conducted on patients with familial benign hypercalcemia and primary hyperparathyroidism were presented in [46], and secondary hyperparathyroidism in [40, 41]. Studies conducted on patients undergoing hemodialysis were presented in [45], hemodialysis with marked secondary hyperparathyroidism in [54], uremic patients on dialysis in [43, 55], and haemodialysis with different forms of renal osteodystrophy in [56] Studies conducted on normal individuals were presented in [57], and hyperparathyroidism patients before and after total parathyroidectomy with autotransplantation were presented in [58]. The above references [40, 41, 43, 45, 46, 54, 55, 56, 57, 58] discussed the similarities and differences in the characteristic features of a reverse sigmoid curve such as the set-point, the slope of the curve at set-point and the maximal or minimal plasma PTH concentration.

The effect of using different methods of calculation on assessment of the set-point in the calcium-PTH reverse sigmoid has been studied in [59]. The dependence of the characteristic features of a reverse sigmoid curve on the rate of change of plasma Ca^{++} was first presented in [38]. Dependence of plasma PTH response on the rate of change of Ca^{++} concentration was also reported in [43, 60, 61]. Next, we describe the current method used to obtain Ca-PTH reverse sigmoid curve in vivo based on the references cited in this section.

4.2 Current method to obtain the Ca-PTH reverse sigmoid curve

The current method of obtaining a Ca-PTH reverse sigmoid curve involves, in general, slowly induced hypo- and hyper-calcemic clamp tests conducted on a set of subjects to obtain plasma Ca^{++} and PTH concentrations measurements at frequent intervals. An example is shown in Figure 4.2 [40]. In this particular example, hypo- and hyper-calcemic clamp tests are

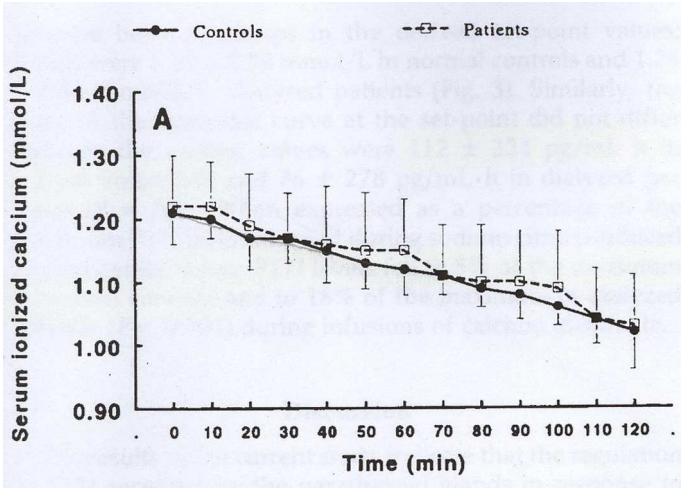

(a) Induced hypocalcemia.

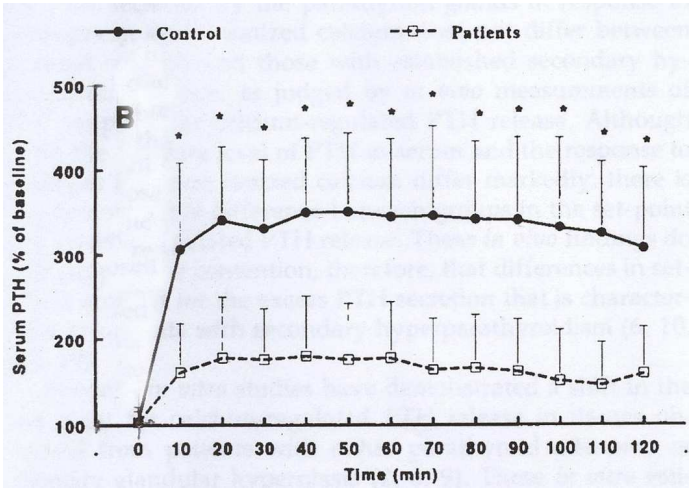

(b) PTH response for induced hypocalcemia.

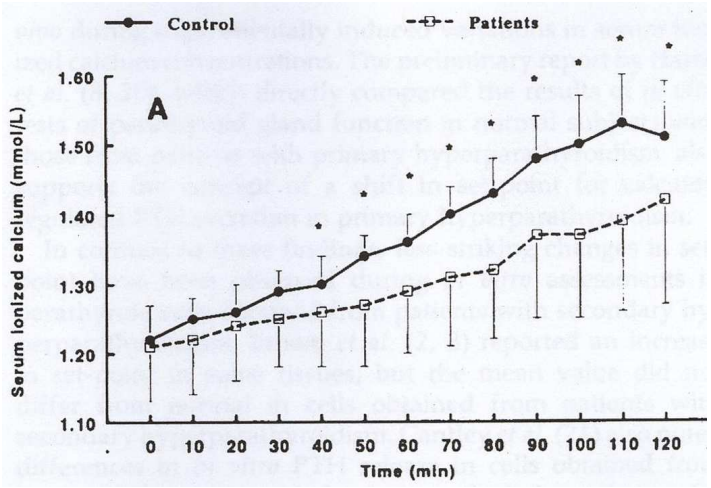

(c) Induced hypocalcemia.

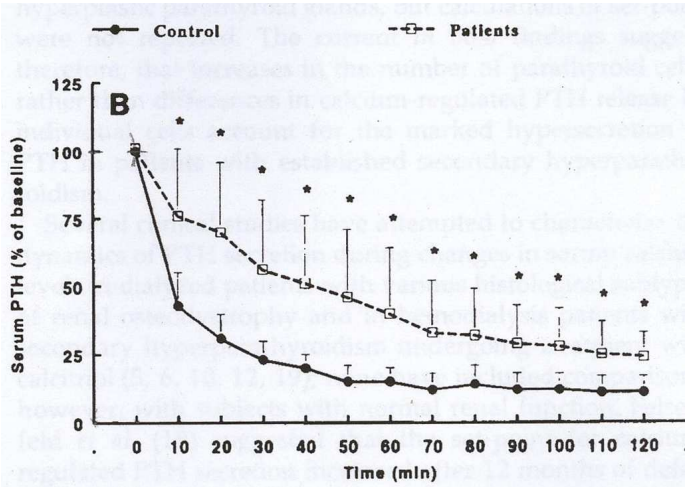

(d) PTH response for induced hypocalcemia.

Figure 4.2. An example of a slowly induced calcemic clamp test. Solid dots represent data of healthy subjects. Squares represent data of patients with secondary hyperparathyroidism. Scanned from [40].

conducted on two sets of subjects: patients with secondary hyperparathyroidism and normal individuals. Plasma Ca^{++} and PTH concentrations are measured every 10 minutes during the test periods of 120 minutes (Figure 4.2). Corresponding plasma Ca^{++} concentration and PTH concentration values of patients with secondary hyperparathyroidism and normal individuals [40] are plotted in Ca-PTH graph to obtain the reverse sigmoid curves as shown in Figure 4.3. Note the differences in the features such as set-point values, slope of the curve

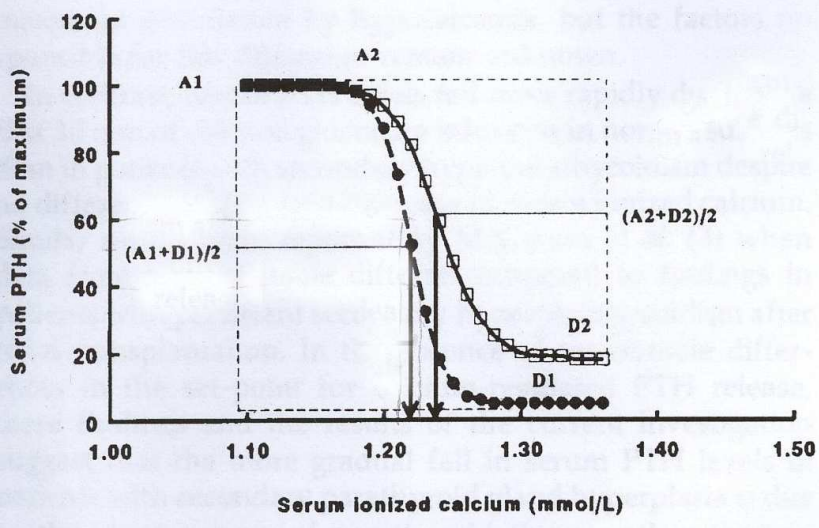

Figure 4.3. A typical calcium-PTH reverse sigmoid curve corresponding to the data shown in Figure 4.2. Solid dots represent data of healthy subjects. Squares represent data of patients with secondary hyperparathyroidism. Scanned from [40].

at the set-point and the minimal saturation values of plasma PTH concentration between the curves obtained for the two sets of subjects. The purpose of this discussion is to give readers an idea of how the Ca-PTH reverse sigmoid curve is obtained. So, we will not get into details of significance of these differences. Next, we present a limitation of the current method to plot Ca-PTH reverse sigmoid curve.

4.3 A limitation of the current method

Taking pairs of points at arbitrary times can lead to a misleading curve. For example, consider a rapidly induced calcemic clamp test [20] as shown in Figure 4.4. The curve obtained by plotting corresponding plasma Ca^{++} and PTH concentrations is not a reverse sigmoid [62] in shape as shown in Figure 4.5. It appears that one cannot select any arbitrary pair of (plasma Ca^{++} concentration, plasma PTH concentration) data points to construct the reverse sigmoid curve. Next, we use our model to analyze this problem of obtaining a meaningful Ca-PTH curve.

4.4 Analysis of simulation results

The model developed in Chapter 3 is described by

$$\begin{pmatrix} \dot{x_1} \\ \dot{x_2} \end{pmatrix} = \begin{pmatrix} -(\lambda_{\mathrm{Ca}}(t) + \lambda_1) & 0 \\ \lambda_{\mathrm{Ca}}(t) & \lambda_2 \end{pmatrix} \begin{pmatrix} x_1 \\ x_2 \end{pmatrix} + \begin{pmatrix} k & 0 \\ 0 & 0 \end{pmatrix} \begin{pmatrix} 1 \\ 0 \end{pmatrix}, \tag{4.2}$$

where

$$\lambda_{\mathrm{Ca}}(t) = \frac{A - B}{1 + \left(\frac{Ca(t)}{S}\right)^m} + B. \tag{4.3}$$

For simulation purposes, the parameter values of the model parameterized for the third subject from Tables 3.7-3.5 are used. Figure 4.6 represents the simulation for induced hypocalcemic clamp test, where $Ca(t) = c_1 + c_2 e^{-\sigma t}$. Plasma Ca^{++} concentration is decreased at a slower rate initially, represented by the profile with σ_1 and subsequently at progressively faster rates, represented by σ_2, and σ_3 as shown in Figure 4.6(a), to a same lower steady-state value ($\sigma_1 < \sigma_2 < \sigma_3$). Note that for the slowest rate calcium input, the corresponding PTH response doesn't show a peak as shown in Figure 4.6(b). But for the faster rate calcium inputs, peaks in the PTH responses are conspicuous. The peak value progressively increases as the calcium input rate becomes faster. A step input produces the maximum value of the

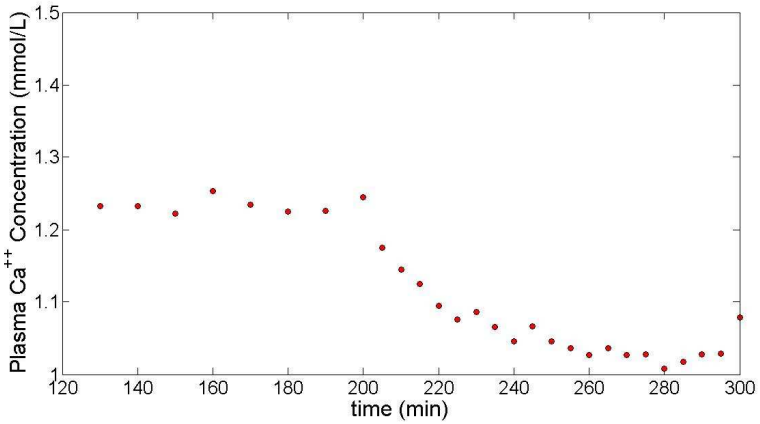

(a) Induced hypocalcemia.

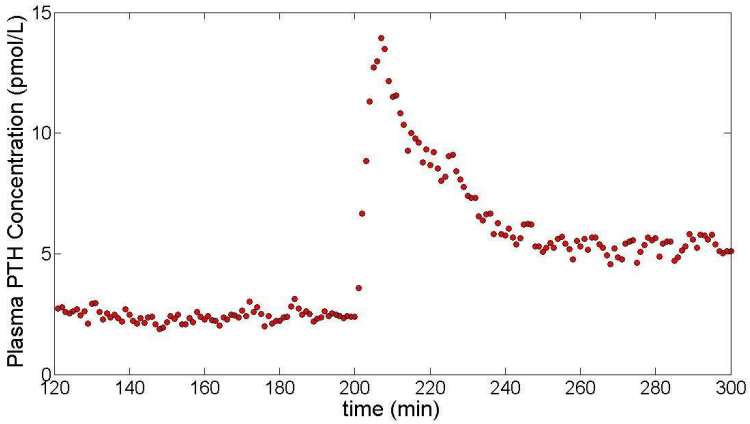

(b) PTH response for induced hypocalcemia.

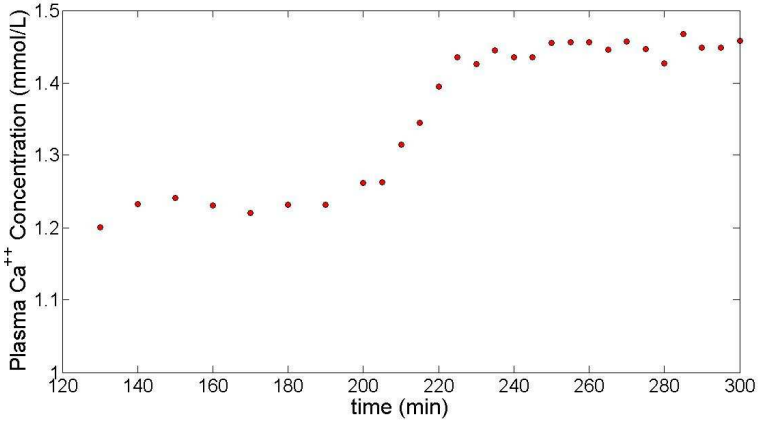

(c) Induced hypocalcemia.

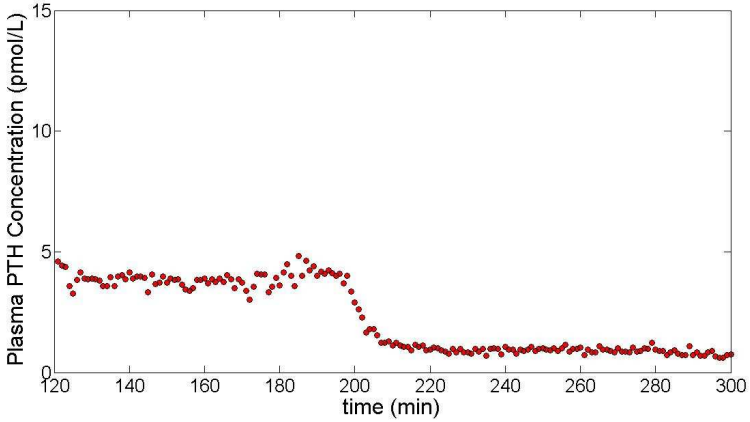

(d) PTH response for induced hypercalcemia.

Figure 4.4. An example of rapidly induced calcemic clamp test [20].

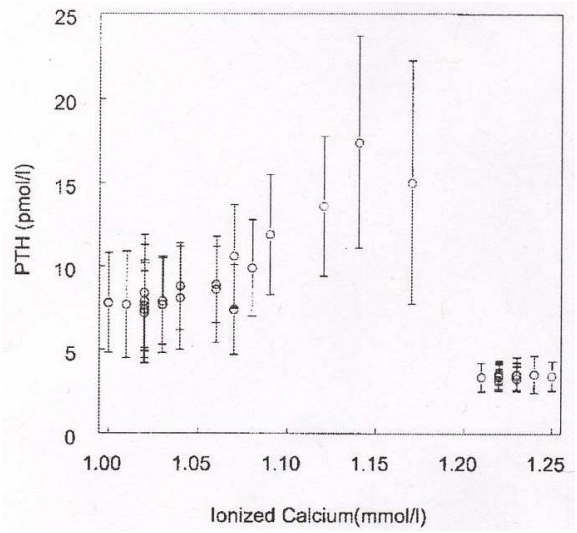

Figure 4.5. A calcium-PTH curve that would result from the conventional approach using data from a rapidly induced calcemic clamp test [20]. This curve doesn't resemble the expected reverse sigmoidal shape. Scanned from [62].

peak and smallest $t_{\max}$. This result is consistent with the observation made in [38] (Figure 4.7) in which hypocalcemia was induced in healthy subjects to attain multiple intermediate steady-states. Same intermediate steady-state of plasma Ca^{++} concentration was achieved at a faster and a slower rate as shown in Figure 4.7(a). The faster decrease in plasma Ca^{++} concentration produced higher peak in the PTH response as shown in Figure 4.7(b). The PTH responses appear to settle at same value after each 30 minutes duration for both faster and slower hypocalcemia induction.

Figure 4.8 represents the simulation of an induced hypercalcemic clamp test where $Ca(t) = c_3 - c_4 e^{-\sigma t}$. Plasma Ca^{++} concentration is increased at a slower rate initially, represented by the profile with σ_1 and subsequently at progressively faster rates, represented by σ_2, and σ_3, as shown in Figure 4.8(a), and eventually to a lower steady-state value ($\sigma_1 < \sigma_2 < \sigma_3$). Note that for the slowest rate calcium input, the corresponding PTH response doesn't show a dip as shown in the Figure 4.8(b). With progressively faster rate calcium inputs, the dips in the PTH responses become more prominent. A step input produces

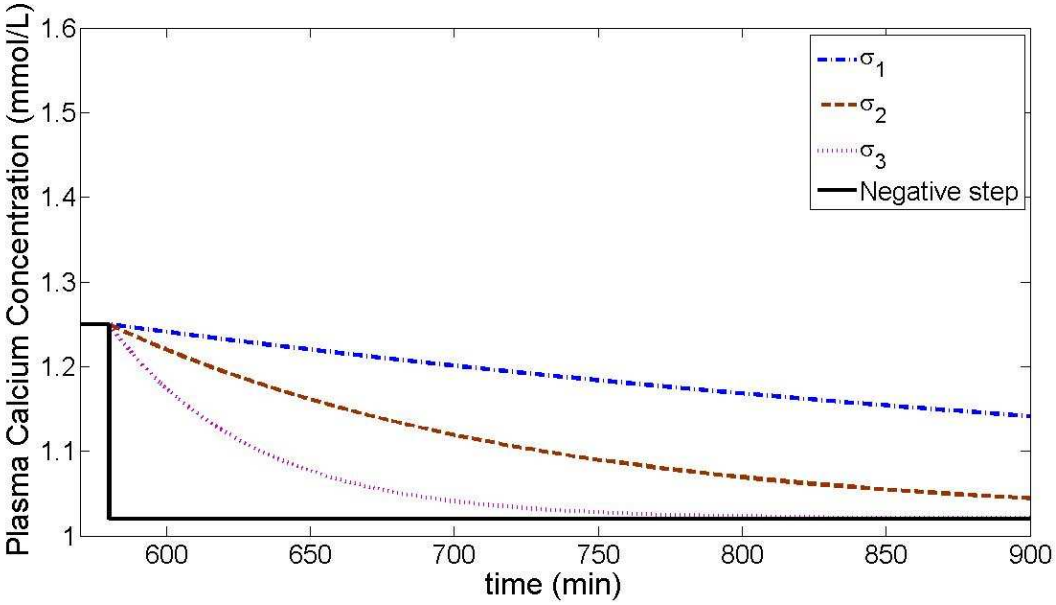

(a) Induced hypocalcemia at varying rates (input). $\sigma_1 < \sigma_2 < \sigma_3$.

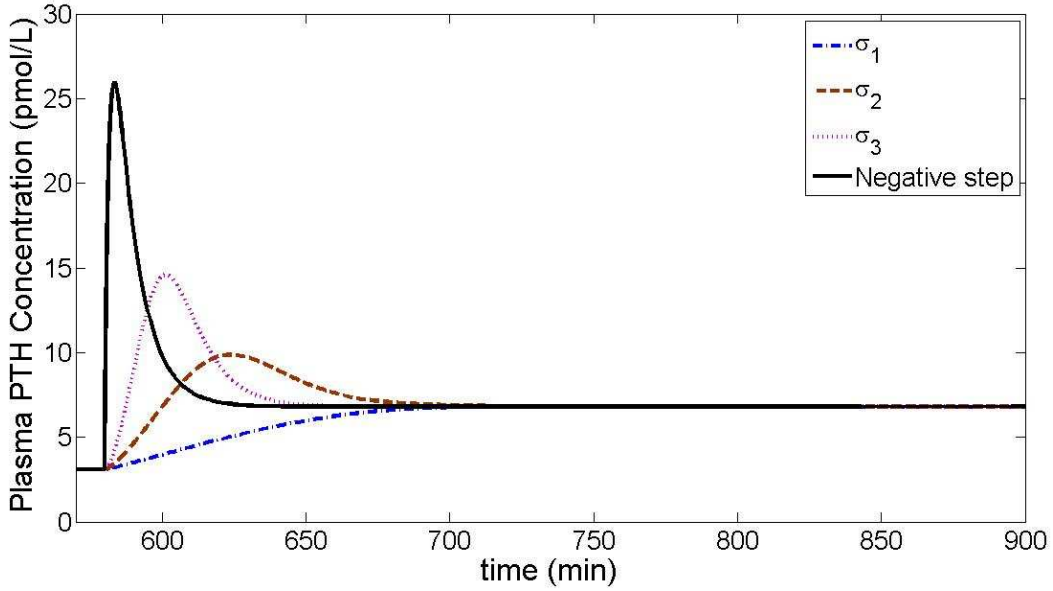

(b) Corresponding PTH response (output).

Figure 4.6. Simulation of PTH response for hypocalcemia induced at varying rates. The model was parameterized using data from healthy subject 3 (Figure 3.14 and Tables 3.5-3.7).

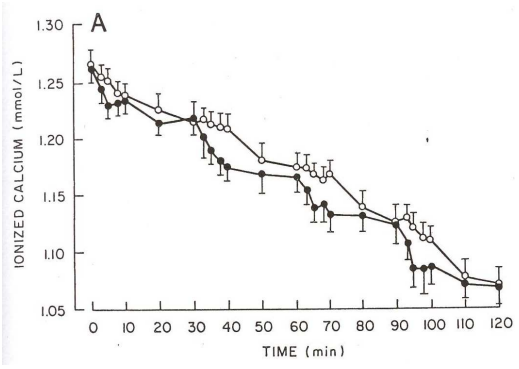

(a) Induced hypocalcemia attaining multiple intermediate steady-states. Same intermediate steady-state of plasma Ca^{++} concentration was achieved at a faster (dots) and a slower (circles) rate.

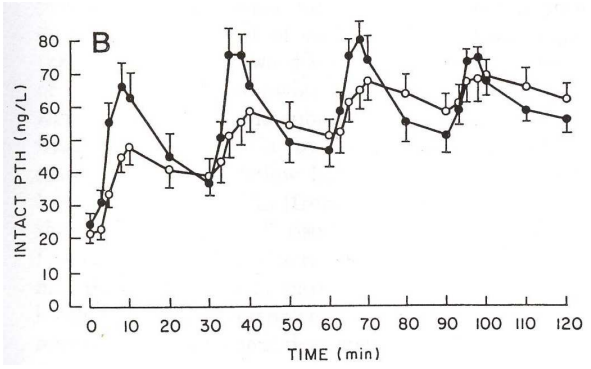

(b) PTH response corresponding to Figure (a). Note the higher peaks in the PTH responses corresponding to faster change in Ca^{++} (dots) and lower peaks corresponding to slower change in Ca^{++} (circles). The responses appear to settle at same value after each 30 minutes duration.

Figure 4.7. An induced hypocalcemic clamp test. Scanned from [38].

the minimum dip value and smallest $t_{\max}$. Unfortunately, we could not find the appropriate published data for comparison. However, one thing seems to be consistent, that is, the dips for PTH response obtained during hypercalcemic clamp tests are not as conspicuous as the peaks obtained during hypocalcemic clamp tests. The simulations shows that even for the fastest (step) increase in plasma Ca^{++} concentration, there isn't a conspicuous dip in the PTH response profile. This is again consistent with the observed clinical data [20] in which plasma Ca^{++} concentration has been raised very fast but the resulting PTH response doesn't show a conspicuous dip (Figure 4.4(c)-(d)).

In addition to issues related to its construction, there appears to be some confusion as to what the reverse sigmoid model actually represents. Some researchers have used it to represent steady-state PTH secretion rate vs steady-state plasma Ca^{++} concentration [33], some researchers have used it to represent PTH secretion rate as a function of plasma Ca^{++} concentration in the dynamical model of the Ca-PTH axis [35], while most have used it to represent relationship between plasma PTH concentration and plasma Ca^{++} concentration

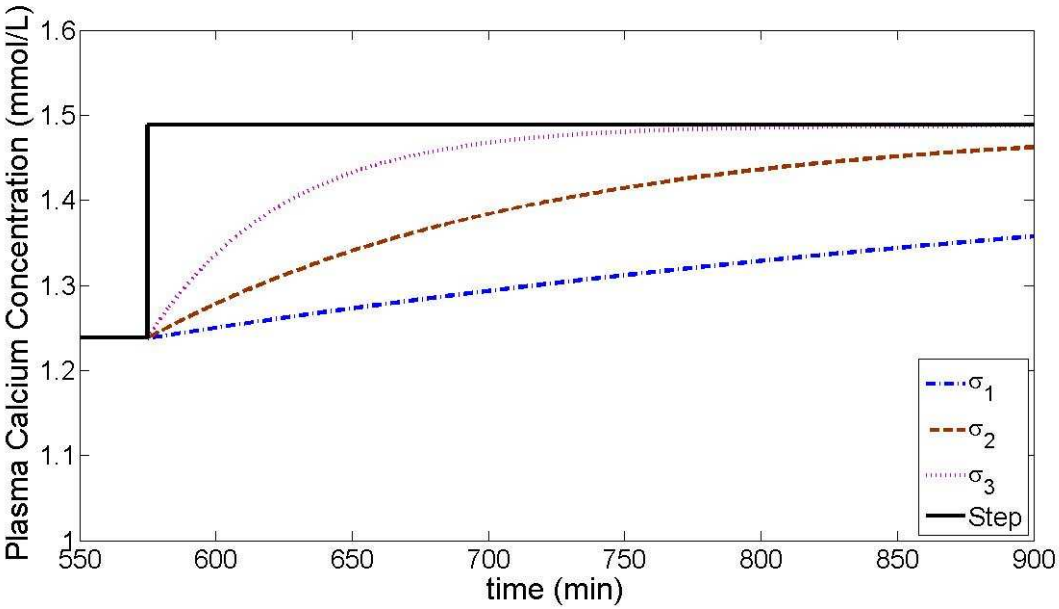

(a) Induced hypercalcemia at varying rates (input). $\sigma_1 < \sigma_2 < \sigma_3$.

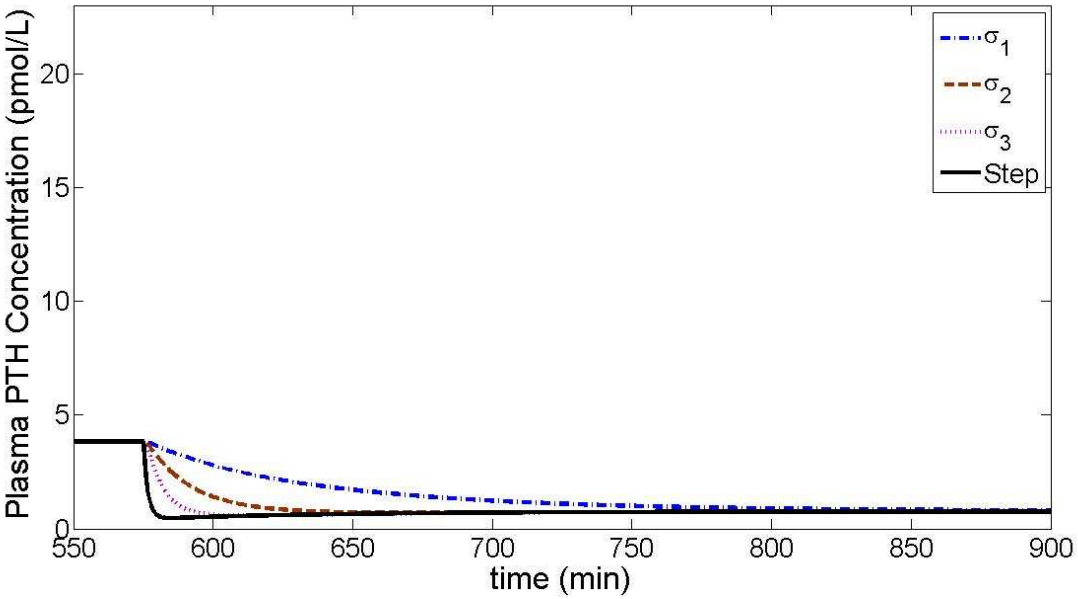

(b) Corresponding PTH response for induced hypocalcemia (output).

Figure 4.8. Simulation of PTH response for hypercalcemia induced at varying rates. The model was parameterized using data from healthy subject 3 (Figure 3.14 and Tables 3.5-3.7).

during induced hypo- and hyper- calcemic clamp test [40, 41, 43, 45, 46, 54, 55, 56, 57, 58, 59]. These papers present clinical studies based on the characteristic features of the reverse sigmoid curve such as the set-point, the slope of the curve at set point, and the maximal or minimal plasma PTH concentrations to find a possible explanation of normal and diseased states of calcium. The method used to plot the reverse sigmoid curve has been presented in Section 4.2. We note that [19] used it to represent the secretion-rate function in the two-pool LTI model. Let us study these differing interpretations using our model. Recalling the steady-state Equations (3.6) and (3.7):

$$\begin{aligned} k &= \left[\frac{A-B}{1+\left(\frac{Ca_{SS}}{S}\right)^m}+B\right]x_{1,SS}+\lambda_1 x_{1,SS}, \\ \lambda_2 x_{2,\mathrm{SS}} &= \left[\frac{A-B}{1+\left(\frac{Ca_{SS}}{S}\right)^m}+B\right]x_{1,SS}, \end{aligned}$$

and using $y = x_{2,\mathrm{SS}}$ (steady-state plasma PTH level) and $x = Ca_{\mathrm{SS}}$ (steady-state plasma Ca^{++} concentration), we get

$$y(x) = \frac{k}{\lambda_2}\left[\frac{1}{1+\frac{\lambda_1}{\frac{A-B}{1+(\frac{x}{S})^m}+B}}\right].$$

Evaluating limits,

$$\begin{aligned} y_{\max} \equiv \lim_{x\to 0}\ y &= \frac{k}{\lambda_2}\left[\frac{1}{1+\frac{\lambda_1}{A}}\right] \\ y_{\min} \equiv \lim_{x\to \infty}\ y &= \frac{k}{\lambda_2}\left[\frac{1}{1+\frac{\lambda_1}{B}}\right]. \end{aligned}$$

Since $A > B$ from the definition of the curve, it follows that, $y_{\max} > y_{\min}$ for all $x \in [0, \infty]$. Next, let us rewrite $y(x)$ as

$$y(x) = \frac{k}{\lambda_2}\left[\frac{1}{1+\frac{\lambda_1}{\frac{A-B}{1+(\frac{x}{S})^m}+B}}\right] = \frac{k}{\lambda_2}\left[\frac{\left(\frac{A-B}{1+(\frac{x}{S})^m}+B\right)}{\left(\frac{A-B}{1+(\frac{x}{S})^m}+B\right)+\lambda_1}\right] = \frac{k}{\lambda_2}\left[\frac{A+\frac{B}{S^m}x^m}{A+\frac{B}{S^m}x^m+\lambda_1+\frac{\lambda_1}{S^m}x^m}\right].$$

Differentiating with respect to x gives

$$\begin{aligned}\frac{dy}{dx} =& \frac{k}{\lambda_2}\frac{d}{dx}\left[\frac{A+\frac{B}{S^m}x^m}{A+\frac{B}{S^m}x^m+\lambda_1+\frac{\lambda_1}{S^m}x^m}\right] \\ =& \frac{k}{\lambda_2}\frac{\left(A+\frac{B}{S^m}x^m+\lambda_1+\frac{\lambda_1}{S^m}x^m\right)\frac{B}{S^m}mx^{m-1}-\left(A+\frac{B}{S^m}x^m\right)\left(\frac{B}{S^m}mx^{m-1}+\lambda_1+\frac{\lambda_1}{S^m}mx^{m-1}\right)}{\left(A+\frac{B}{S^m}x^m+\lambda_1+\frac{\lambda_1}{S^m}x^m\right)^2} \\ =& -\frac{k}{\lambda_2}\frac{(A-B)\frac{\lambda_1}{S^m}mx^{m-1}}{\left(A+\frac{B}{S^m}x^m+\lambda_1+\frac{\lambda_1}{S^m}x^m\right)^2}.\end{aligned}$$

Since $(A-B)>0$ and $A,\ B,\ k,\ x,\ \lambda_1,\ \lambda_2,\ S,\ m>0$, it follows that $\frac{dy}{dx}<0$. Thus, $y(x)$ is a monotonically decreasing function. Since we already showed that $y(x)$ is bounded above by $y_{\max}$ and bounded below by $y_{\min}$, the model implies that a reverse sigmoidal relationship exists between plasma Ca^{++} and PTH concentrations at steady-state. Now if we consider that the reverse sigmoid relationship represents the model for PTH secretory rate as a function of plasma Ca^{++} concentration as in [33, 35], the dynamical model for the rate of change of plasma PTH concentration from Section 3.3 becomes

$$\dot{x_2}(t) = \underbrace{\frac{\mathrm{A}-\mathrm{B}}{1+\left(\frac{Ca}{\mathrm{S}}\right)^{\mathrm{m}}}+\mathrm{B}}_{\text{Secretion to plasma from parathyroid gland}} \underbrace{-\lambda_2 x_2(t).}_{\text{Clearance}}$$

Note that the system has been reduced into single pool model. For $x_2(t_0)=0$ at $t_0=0$, the

solution of the above system is given by

$$x_2(t) = \int_{t_0}^{t} \left(\frac{\mathrm{A} - \mathrm{B}}{1 + \left(\frac{Ca(t)}{\mathrm{S}}\right)^{\mathrm{m}}} + \mathrm{B} \right) \mathrm{e}^{-\lambda_2 \sigma} \, d\sigma \;\; , t \geq t_0, \;\; x_2(t_0) = 0, \;\; t_0 = 0.$$

Considering a step decrease in calcium

$$\begin{aligned} Ca(t) &= Ca, \; t < t_0 \\ &= 0, \; t \geq t_0 \end{aligned}$$

the solution can be simplified to

$$x_2(t) = \left(\frac{\mathrm{A} - \mathrm{B}}{1 + \left(\frac{Ca}{\mathrm{S}}\right)^{\mathrm{m}}} + \mathrm{B} \right) \int_{t_0}^{t} \mathrm{e}^{-\lambda_2 \sigma} \, d\sigma = \left(\frac{\mathrm{A} - \mathrm{B}}{1 + \left(\frac{Ca}{\mathrm{S}}\right)^{\mathrm{m}}} + \mathrm{B} \right) \left(\frac{1 - \mathrm{e}^{-\lambda_2 t}}{\lambda_2} \right).$$

Here, due to $(1 - \mathrm{e}^{-\lambda_2 t})$, the time profile of the solution always looks like Figure 3.3(b) and can never exhibit the peak shown in Figure 3.3(c). But we know from the clinical data in [20, 38] that even much slower changes in plasma Ca^{++} result in plasma PTH responses as shown in Figure 3.3(c).

Based on above analysis, we conclude that the reverse sigmoid model should not be used to represent the secretion rate as a function of plasma Ca^{++} concentration in the dynamical model for calcium-PTH axis. In fact, the reverse sigmoid relationship presented in [33] is nothing but the curve fitting done for approximated steady-state values of Ca^{++} and corresponding PTH secretion rates in vitro. Moreover, the clinical studies based on the characteristic features of the reverse sigmoid curve such as the set-point, the slope of the curve at set point and the maximal or minimal plasma PTH concentrations to find a possible explanation of normal and diseased states of calcium homeostasis in [40, 41, 43, 45, 46, 54, 55, 56, 57, 58, 59] used transient data to construct the curve, rendering the results questionable.

We also noted that PR Conlin with his colleagues including EM Brown reported hysteresis in the relationship between plasma Ca^{++} and PTH concentration [39] using transient data. Since a hysteresis curve should represent only the steady-state values [63, 64], the reported hysteresis is questionable. Hysteresis of PTH response to hypocalcemia in hemodialysis patients with bone disease was reported in [42, 53]. Unfortunately, this claim was also based on the transient data. Next, we propose a new protocol to construct a Ca-PTH reverse sigmoid curve to overcome the limitations of present procedures.

4.5 The new protocol

Consider the three asymptotes L_1, L_2, and L_3 in the Ca-PTH reverse sigmoid curve as shown in Figure 4.9:

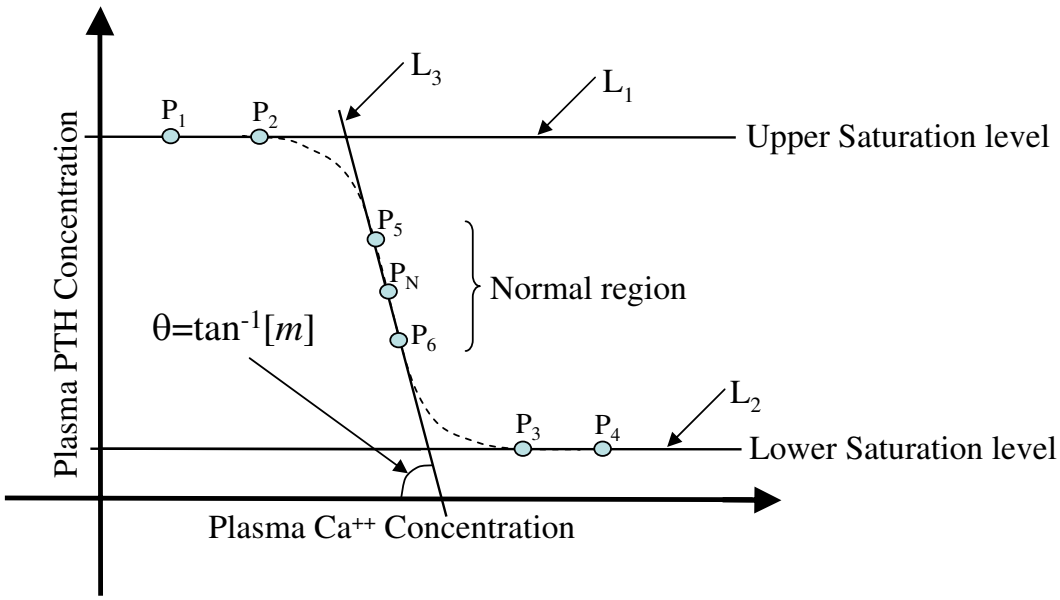

Figure 4.9. Constructing the Ca-PTH reverse sigmoid curve.

1. Asymptote L_1 passing through the upper saturation level,

2. asymptote L_2 passing through the lower saturation level, and

3. asymptote L_3 passing through the normal region.

We need at least 2 points to define each of these asymptotes. Therefore, a minimum of 6 points are required to construct a working reverse sigmoid curve. Induced hypocalcemic clamp tests should be conducted to obtain three steady-state data points P_1, P_2, and P_5 and induced hypercalcemic clamp tests should be conducted to obtain three steady-state data points P_3, P_4,and P_6. Note that P_5 and P_6 should be very close to P_N corresponding to the normal plasma Ca^{++} and PTH concentration values. Assuming that the curve is linear in this neighborhood, they define L_3.

In conclusion, we state that:

1. reverse sigmoid model should not be used to represent the secretion rate in the dynamical model of calcium-PTH axis, but should only be used to represent the secretion rate function,

2. only steady-state data should be used in plotting Ca-PTH reverse-sigmoid curve to obtain consistent result and meaningful interpretation,

3. only steady-state data should be used in the investigation of possible hysteresis in relationship between plasma PTH and Ca^{++} concentrations, and

4. if transient data are used, then the resulting curve becomes dependent on the particular subject's axis dynamics or the calcemic clamp test procedure rendering such studies unreliable. Transient data can be useful only to study the overall dynamic response of plasma PTH to the changes in plasma Ca^{++} concentration.

CHAPTER 5

CONCLUSIONS

In this thesis a two-pool, linear, time-varying model was developed to describe the acute Ca-PTH axis dynamics. This model, parameterized based on clinical data from hypocalcemic clamp test successfully predicted PTH response for hypercalcemic clamp test in healthy humans. Using analysis and simulation, we proposed a new protocol for the construction of the Ca-PTH reverse sigmoid curve, an integral part of this model. The proposed protocol overcomes limitations of current procedures in that it is independent of the particular subject's axis dynamics or the manner by which the calcemic clamp test is conducted. This model is a good candidate for inclusion in an overall calcium homeostasis model that may be used to study the health and disease associated with calcium homeostasis.

BIBLIOGRAPHY

[1] JM Bruder, TA Guise, and GR Mundy. *Endocrinology and metabolism*, chapter Mineral metabolism, pages 1079–1177. McGraw-Hill, New York, 4th edition, 2001.

[2] T Gunther and G Karsenty. *Molecular biology of the parathyroid*, chapter Development of parathyroid glands, pages 1–7. Kluwer Acedemic/Plenum, New York, 1st edition, 2005.

[3] AC Looker, ES Orwoll, CC Johnston Jr., RL Lindsay, HW Wahner, WL Dunn, MS Calvo, TB Harris, and SP Heyse. Prevalence of low femoral bone density in older U.S. adults from NHANES III. *Journal of Bone and Mineral Research*, 12:1761–1768, 1997.

[4] National Osteoporsis Foundation. http://www.nof.org/osteoporosis/diseasefacts.htm. Fast facts on osteoporosis.

[5] Institute for system biology. http://www.systemsbiology.org/Intro_to_ISB_and_Systems_BiologySystems_Biology__the_21st_Century_Science. Systems biology-the 21st century science.

[6] HS Wiley. System biology beyond the buzz: Lesson from EGFR reseach show how to kick-start a systems approach for other areas of biology. *The Scientist*, 20:53–57, 2006.

[7] SS Nussey and SA Whitehead. *Endocrinology an integrated approach.* BIOS, Oxford, 1st edition, 2001.

[8] D Shoback, R Marcus, and D Bikle. *Basic & clinical endocrinology*, chapter Metabolic bone disease, pages 295–361. Lange Medical Books/McGraw-Hills, New York, 7th edition, 2004.

[9] AF Stewart and AE Broadus. The regulation of renal calcium excretion: An approach to hypercalciuria. *Annual Review of Medicine*, 32:457–473, 1981.

[10] G Jones, SA Strugneli, and HF DeLuca. Current understanding of the molecular actions of vitamin D. *Physiological Reviews*, 78:1193–1231, 1998.

[11] VA LiVolsi. *The parathyroids basic and clinical concepts*, chapter Embryology, anatomy, and pathology of the parathyroids, pages 1–14. Academic Press, New York, 1st edition, 1994.

[12] VC Scanlon and T Sanders. *Essentials of anatomy and physiology*, chapter The endocrine system. F. A. Davis Company, Philadelphia, 5th online edition, 2007.

[13] MSH diFiore. *Atlas of normal histology*, chapter Endocrine system, pages 202–203. Lea and Febiger, Philadelphia, 6th edition, 1989.

[14] JF Habener. Regulation of parathyroid hormone secretion and biosynthesis. *Ann. Rev. Physiol.*, 43:211–223, 1981.

[15] GN Gill. *Endocrinology and metabolism*, chapter Biosynthesis, secretion and metabolism of hormones, pages 29–48. McGraw-Hill, New York, 4th edition, 2001.

[16] S Yano and EM Brown. *Molecular biology of the parathyroid*, chapter The calcium sensing receptor, pages 44–56. Kluwer Acedemic/Plenum, New York, 1st edition, 2005.

[17] T Naveh-Many and J Silver. *Moecular biology of the parathyroid*, chapter Regulation of parathyroid hormone gene expression by 1,25-dihydroxyvitamin D, pages 84–94. Kluwer Academic/Plenum Publishers, New York, 1st edition, 2005.

[18] R Kilav, J Silver, and T Naven-Many. *Molecular biology of the parathyroid*, chapter Regulation of parathyroid hormone mRNA stability by calcium and phosphate, pages 57–67. Kluwer Academic/Plenum Publishers/Landes Bioscience/Eurekah.com, New York, 1st edition, 2005.

[19] G Momsen and P Schwarz. A mathematical/physiological model of parathyroid hormone secretion in response to blood-ionized calcium lowering in vivo. *Scan J Clin Lab Invest*, 57:381–394, 1997.

[20] CP Schmitt, F Schaefer, A Bruch, JD Vel, H Schmidt-Gayk, G Stein, E Ritz, and O Mehls. Control of pulsatile and tonic parathyroid hormone secretion by ionized calcium. *Journal of Clinical Endocrinology and Metabolism*, 81:4236–4243, 1996.

[21] MH Kroll. Parathyroid hormone temporal effects of bone formation and resorption. *Bulletin of Mathematical Biology*, 62:163–187, 2000.

[22] LK Potter, LD Greller, CR Cho, ME Nuttall, GB Stroup, LJ Suva, and FL Tobin. Response to continuous and pulsatile PTH dosing: A mathematical model for parathyroid hormone receptor kinetics. *Bone*, 37:159–169, 2005.

[23] L Jin, AH Tashjian, and F Zhang. *Molecular biology of the parathyroid*, chapter Towards an understanding of human parathyroid hormone structure and function, pages 29–43. Kluwer Academic/Plenum Publishers/Landes Bioscience/Eurekah.com, New York, 1st edition, 2005.

[24] MH Kroll. Modeling the interaction between osteoblast and osteoclast activities in bone remodeling. *Journal of Theoretical Biology*, pages 293–309.

[25] JP Aubert, F Bronner, and LJ Richelle. Quantitation of calcium metabolism theory. *Journal of Clinical Investigation*, 42:885–897, 1963.

[26] L Danziger and GL Elmergreen. Calcium and phosphorus homeostasis in parathyroidectomized dog: Evaluation by means of ethylenediaminetetra-acetate and calcium tolerance test. *J. Clin. Invest*, 39:662–670, 1960.

[27] J Aubert and F Bronner. A symbolic model for the regulation by bone metabolism of the blood calcium level in rats. *Biophysical Journal*, 5:349–358, 1965.

[28] DH Copp. Endocrine regulation of calcium metabolism. *Annual Reviews*, 32:61–86, 1970.

[29] DS Riggs. *Control theory and physiological feedback mechanism*, chapter Parathyroid hormone-plasma calcium, pages 489–496. The Williams and Wilkins Co., Baltimore, MD, 1970.

[30] T. Powell. A mathematical model for calcium homeostasis. *Bulletin of Mathematical Biophysics*, 34:483–502, 1972.

[31] S Hurwitz, S Fishman, A Bar, M Pines, G Riesenfeld, and H Talpaz. Simulation of calcium homeostasis: Modeling and parameter estimation. *American Journal of Physiology*, 245:R664–R672, 1983.

[32] S Hurwitz, S Fishman, and H Talpaz. Model of plasma calcium regulation: System oscillation induced by growth. *American Journa of Physiology*, 252:R1173–R1181, 1987.

[33] EM Brown. Four-parameter model of the sigmoidal relationship between parathyroid hormone release and extracellular calcium concentration in normal and abnormal parathyroid tissue. *Journal of Clinical Endocrinology and Metabolism*, 56:572–581, 1983.

[34] H El-Samad, JP Goff, and M Khammash. Calcium homeostasis and parturient hypocalcemia: An integral feedback perspective. *Journal of Theoretical Biology*, 214:17–29, 2002.

[35] JF Raposo, LG Sobrinho, and HG Ferreira. A minimal mathematical model of calcium homeostasis. *The Journal of Clinical Endocrinology and Metabolism*, 77:4330–4340, 1993.

[36] J D Veldhuis, ML Carlson, and ML Johnson. The pituitary gland secretes in bursts: Appraising the nature of glandular secretory impulses by simultaneous multiple-parameter deconvolution of plasma hormone concentrations. *Proc. Natl. Acad. Sci*, 84:7686–7690, 1987.

[37] MH Samuels, J Veldhuis, C Cawley, RJ Urban, M Luther, R Bauer, and G Mundy. Pulsatile secretion of parathyroid hormone in normal young subjects: Assessment by deconvolution analysis. *Journal of Clinical Endocrinology and Metabolism*, 57:399–403, 1997.

[38] FD Grant, PR Conlin, and EM Brown. Rate and concentration dependence of parathyroid hormone dynamics during stepwise changes in serum ionized calcium in normal humans. *Journal of Clinical Endocrinology and Metabolism*, 71:370–378, 1990.

[39] PR Conlin, VT Fajtova, RM Mortensen, MS LeBoff, and EM Brown. Hysteresis in the relationship between serum ionized calcium and intact parathyroid hormone during recovery from induced hyper-and hypocalcemia in normal humans. *Journal of clinical endocrinology and Metabolism*, 69:593–599, 1989.

[40] JA Ramirez, WG Goodman, J Gornbein, C Menezes, L Moulton, GV Segre, and IB Salusky. Direct in vivo comparision of calcim-regulated parathyroid hormone secretion in normal volunteers and patients with secondary hyperparathyroidism. *Journal of clinical endocrinology and Metabolism*, 76:1489–1494, 1993.

[41] WG Goodman, JD Veldhuis, TR Belin, AJV Herle, H Juppner, and IB Salusky. Calcium-sensing by parathyroid glands in secondary hyperparathyroidism. *Journal of clinical endocrinology and metabolism*, 83:2765–2772, 1998.

[42] AJ Felsenfeld, M Rodriguez, and E Aguilera-Tejero. Dynamics of parathyroid hormone secretion in health and secondary hyperparathyroidism. *Clin J Am Soc Nephrol*, 2:1283–1305, 2007.

[43] V DeCristofaro, C Colturi, A Masa, M Comelli, and LA Pedrini. Rate dependence of acute PTH release and association between basal plasma calcium and set point of calcium-PTH curve in dialysis patients. *Nephrology Dialysis Transplatation*, 16:1214–1221, 2001.

[44] Wikipedia.com. http://en.wikipedia.org/wiki/Blood. Blood.

[45] MJ Borrego, AJ Felsenfeld, A Martin-Malo, Y Almaden, MT Concepcion, P Aljama, and M Rodriguez. Evidence for adaptation of the entire PTH-calcium curve to sustained changes in the serum calcium in hemodialysis patients. *Nephrology Dialysis Transplantation*, 12:505–513, 1997.

[46] S Khosla, PR Ebeling, AF Firek, MM Burritt, PC Kao, and H Heath, III. Calcium infusion suggests a "set-point" abnormality of parathyroid gland function in familial benign hpercalcemia and more complex disturbance in primary hyperparathyroidism. *Journal of Clinical Endocrinology and Metabolism*, 76:715–720, 1993.

[47] JW Blum, GP Mayer, and JT Potts Jr. Parathyroid hormone response during spontaneous hypocalcemia and induced hypercalcemia in cows. *Endocrinology*, 95:84, 1974.

[48] GP Mayer and JG Hurst. Sigmoidal relationship between parathyroid hormone secretion rate and plasma calcium concentration in calves. *Endocrinology*, 102:1036–1042, 1978.

[49] EM Brown, MF Brennan, S Hurwitz, R Windeck, SJ Marx, AM Spiegel, JO Koehler, DG Gardner, and GD Aurbach. Dispersed cells prepared from human parathyroid glands: Distinct calcium sensitivity of adenomas vs. primary hyperplasia. *Journal of Clinical Endocrinology and Metabolism*, 46:267–275, 1978.

[50] EM Brown, DG Gardner, MF Brennan, SJ Marx, AM Spiegel, MF Attie, RW Downs Jr., JL Doppman, and GD Aurbach. Calcium-regulated parathyroid hormone release in primary hyperparathyroidism studies in vitro with dispersed parathyroid cells. *The American Journal of Medicine*, 66:923–931, 1979.

[51] EM Brown, RE Wilson, JG Thacher, and SP Marynick. Abnormal calcium-regulated PTH release in normal parathyroid tissue from patients with adenoma. *The American Journal of Medicine*, 71:565–570, 1981.

[52] EM Brown, RE Wilson, JG Thacher, and SP Marynick. Abnoral regulation of parathyroid hormone release by calcium in secondary hyperparathyroidism due to chronic renal failure. *Journal of Clinical Endocrinology and Metabolism*, 54:172–179, 1982.

[53] AJ Felsenfeld, D Ross, and M Rodriguez. Hysresis of the parathyroid hormone response to hypocalcemia in hemodialysis patients with low turnover Aluminim bone disease. *J Am Soc Nephrol*, 2:1136–1143, 1991.

[54] AJ Felsenfeld, A Jara, M Pahl, J Bover, and M Rodriguez. Difference in the dymamics of parathyroid hormone secretion in hemodialysis patients with marked secondary hyperparathroidism. *Journal of the Aamerican Society of Nephrology*, 6:1371–1378, 1995.

[55] VD Cristofaro, F Sama, B Pagliari, C Colturi, A Sidoti, A Massa, M Filippini, M Comelli, and L Pedrini. Calcium-PTH relationship in dialysis patients, the pitfalls of using a constant dialysate caclium concentration during the dynamic tests. *Clin-Nephrol*, 49(2):113–20, 1998.

[56] AJ Felsenfeld, M Rodriguez, R Dunlay, and F Llach. A comparison of parathyroid-gland function in haemodialysis patients with different forms of renal osteodystrophy. *Nephrology Dialysis Transplant*, 6:244–251, 1991.

[57] P D'Amour, A Rakel, JH Brossard, L Rousseau, C Albert, and T Cantor. Acute regulation of circulating parathyroid hormone (PTH) molecular forms by calcium: Utility of pth fragments/PTH (1-84) ratios derived from three generations of PTH assays. *Journal of Clinical Endocrinology and Metabolism*, 91(1):283–289, 2006.

[58] MCM de Castro and V Jorgetti. Assessment of parathyroid hormone secretion before and after total parathyroidectomy with autotransplantation. *Nephrol Dial Transplant*, 14:2264–2265, 1999.

[59] P Messa, D Turrin, G Mioni, and A Cruciatti. Impact of the method of calculation on assessment of the PTH-calcium set-point. *Nephrology Dialysis Transplantation*, 12:101–105, 1997.

[60] P Schwarz. Dose response dependency in regulation of acute PTH (1-84) release and suppression in normal humans: A citrate and calcium infusion study. *Scand J Clin Lab Invest*, 53:601–605, 1993.

[61] Moyses RMA, Pereira RC, Reis LMD, Sabbaga E, and Jorgetti V. Dynamic tests of parathyroid hormone secretion using hemodialysis and calcium infusion cannot be compared. *Kidney International*, 5:659–665, 1999.

[62] CP Schmitt and F Schaefer. Calcium sensitivity of the parathyroid in renal failure: Another look with new methodology. *JourNephrol Dial Transplant*, 14:2815–2818, 1999.

[63] SH Strogatz. *Nonlinear dynamics and chaos*, chapter Bifurcations, pages 44–92. Westview Press, Massachusetts, 1st edition, 1994.

[64] HD Young, RA Freedman, TR Sandin, and AL Ford. *University physics*, chapter Sources of magnetic field, pages 903–940. Addison Wesley Longman, New York, 10th edition, 2000.